Signatures of a parity-violating universe

William R. Coulton,[1,*] Oliver H. E. Philcox,[2,3,†] and Francisco Villaescusa-Navarro[1,4,‡]
[1]Center for Computational Astrophysics, Flatiron Institute, 162 5th Avenue, New York, New York 10010, USA
[2]Center for Theoretical Physics, Columbia University, New York, New York 10027, USA
[3]Simons Society of Fellows, Simons Foundation, 160 5th Avenue, New York, New York 10010, USA
[4]Department of Astrophysical Sciences, Princeton University, 4 Ivy Lane, Princeton, New Jersey 08544, USA

(Received 21 June 2023; accepted 8 January 2024; published 29 January 2024)

What would a parity-violating universe look like? We present a numerical and theoretical study of mirror asymmetries in the late universe, using a new suite of N-body simulations: QUIJOTE-ODD. These feature parity-violating initial conditions, injected via a simple ansatz for the imaginary primordial trispectrum and evolved into the nonlinear regime. We find that the realization-averaged power spectrum, bispectrum, halo mass function, and matter PDF are not affected by our modifications to the initial conditions, deep into the nonlinear regime, which we argue arises from rotational and translational invariance. In contrast, the parity-odd trispectrum of matter (measured using a new estimator), shows distinct signatures proportional to the parity-violating parameter, $p_{\rm NL}$, which sets the amplitude of the primordial trispectrum; furthermore, the statistic cannot be sourced by any conventional gravitational or baryonic processes. We additionally find intriguing signatures in the angular momentum of halos, with the primordial trispectrum inducing a nonzero correlation between angular momentum and smoothed velocity field, proportional to $p_{\rm NL}$. Our simulation suite has been made public to facilitate future analyses.

DOI: 10.1103/PhysRevD.109.023531

I. INTRODUCTION

Parity describes the transformation properties of a system under point reflections; roughly speaking, a symmetric universe is one that looks identical when left and right are exchanged. From a terrestrial viewpoint, violations of this symmetry are commonplace: examples include neutrinos (which are solely left handed), amino acid chirality, and the handedness of the brain. Physically, many of these effects are sourced by the weak interaction, which, as discovered empirically in 1957 [1,2], does not obey parity symmetry (unlike other standard model forces), but rather the more general symmetry of charge-parity-time conservation.

More broadly, one may ask whether parity-symmetry should be broken also on cosmological scales. In this instance, physics is dominated not by the weak force but by gravitation, which is invariant under reflections (in the Einsteinian paradigm). As such, a bound on large-scale parity asymmetries provides a probe of the Universe's initial conditions. In the simplest models of inflation, single-field slow-roll, parity symmetries are obeyed [3,4]; however, violation can occur as a result of exotic physics, which would indicate phenomena such as new forces, interactions with novel particles, or loop corrections [5–14]. Indirect evidence for mirror asymmetries may already exist; the known asymmetry of baryons over antibaryons requires a charge-parity- and charge-violating process, as described by the Sakharov conditions [15], which could occur via some form of gravitational parity violation [16–19].

Ascertaining whether the Universe is parity symmetric is a topic of particular current relevance. Using data from large spectroscopic surveys, recent works have revealed a slight asymmetry in the distribution of chiral tetrahedra of galaxies [20,21], using a method first presented in [22]. Whilst it is important to bear in mind that various systematic effects could cause this result, there remains an intriguing possibility that this signal is physical. As discussed above, this could indicate parity-violating processes at work in inflation or at late times (e.g., via some flavor of chiral gravity), though the latter requires an exceedingly large characteristic length scale [23]. As shown in [24], the former explanation is also disfavored, since the relevant signal does not show up in the cosmic microwave background (CMB) trispectrum, where it would be expected to arise at some 50σ (under some limiting assumptions, such as approximate scale invariance). This suggests that systematics (mischaracterization of noise in particular), may be to blame. Future data will shed much more light on such results, and there remains the possibility

*wcoulton@flatironinstitute.org
†ohep2@cantab.ac.uk
‡fvillaescusa@flatironinstitute.org

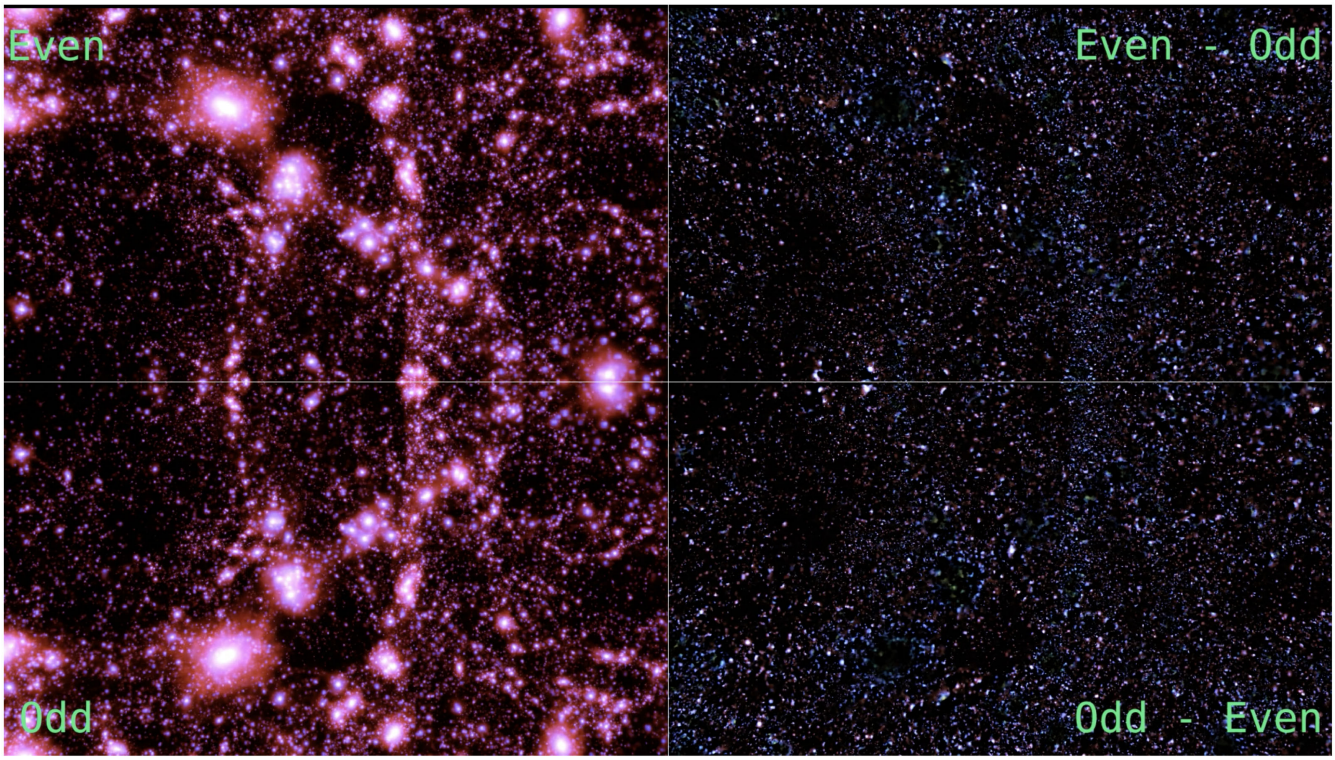

FIG. 1. We show two N-body simulations: one with standard initial conditions (top left) and one with parity-violating initial conditions (bottom left) with $p_{\rm NL} = 10^7$. Both simulations follow the evolution of 512^3 particles on a periodic volume of $(50h^{-1}\,{\rm Mpc})^3$ down to $z = 0$, and they share the same underlying Gaussian density field. The parity-violating simulation has been flipped along the horizontal axis to give the impression that there is a mirror at the center of the image. The panels on the right part show the difference between the densities of the two simulations. As can be seen, parity violating induces non-negligible differences in the distribution of matter in the Universe, the statistical implications of which will be discussed in this work. The images are generated from a full ray-tracing calculation at redshift zero from blender.

that robust signatures could be detected with future surveys such as DESI, Euclid, MegaMapper and beyond [e.g., [25–27]].

If an early-Universe source of parity violation exists, how best can it be searched for? Put another way: how do mirror asymmetries in inflation manifest themselves in the distribution of matter and galaxies today? Previous observational studies have principally focused on the four-point correlation function or trispectrum (though see also [28,29]), which, in the linear regime, directly probes the (parity-sensitive) primordial trispectrum of inflation. At late times however, the Universe is significantly more complex due to nonlinear gravitational evolution. Does this leak information into lower-point functions? Or change the masses of galaxies? Or their angular momenta? To probe such effects, we require numerical codes to simulate gravitational effects down to redshift zero and thus assess the impact on cosmological statistics such as power spectra, halo mass functions, and beyond.

In this work, we will present the first numerical study of cosmologies with primordial scalar parity violation. To this end, we will consider the generation of asymmetric initial conditions from a fiducial template and generate their low redshift counterparts, creating an extension to the QUIJOTE suite [30], dubbed QUIJOTE-ODD. By way of introduction, we show a slice through an analogous (enlarged) simulation in Fig. 1, comparing to its parity-even counterpart; an associated movie can be found online.[1] Using these realizations, we can robustly compute the late-time manifestations of parity-violating initial conditions and compare them to theoretical predictions, made possible in part by novel trispectrum estimators. Here, we will consider a range of statistics: the power spectrum, bispectrum, trispectrum, halo mass function, matter PDF, and halo angular momentum statistics. Each will be measured from both parity-conserving and parity-violating simulations, which will allow us to test theoretical expectations and uncover various future avenues for exploration.

The remainder of this work is as follows. We begin with a general introduction to scalar parity violation, presenting theoretical arguments for the parity sensitivity of various observables in Sec. II. In Sec. III, we consider how to

[1]Movie available at www.youtube.com/watch?v=4bnKGFYoLpA&t=2s&ab_channel=FranciscoVillaescusa-Navarro.

generate parity-violating initial conditions, before Sec. IV discusses the associated simulation suite. Section V shows results of various correlators extracted from our simulations, and compares to theoretical predictions, before we conclude in Sec. VI, with Appendixes A and B discussing mathematical minutiae pertaining to trispectrum estimation and theory modeling.

II. PARITY VIOLATION IN THEORY

A. Definition

Consider a scalar function, ζ, depending on n displacement vectors $\mathbf{r}_1, \ldots, \mathbf{r}_n$. The action of a three-dimensional parity transformation, denoted $\mathbb{P}$, is the following:

$$\mathbb{P}[\zeta(\mathbf{r}_1, \ldots, \mathbf{r}_n)] = \zeta(-\mathbf{r}_1, \ldots, -\mathbf{r}_n), \tag{1}$$

which is equivalent to a point reflection. If $\mathbb{P}[\zeta] = \pm\zeta$, we describe the statistic as parity even or parity odd respectively. Assuming isotropy, the scalar function ζ can depend only on the position vectors r_i^a, derivatives ∂^a, and rotationally invariant quantities, i.e. δ_{K}^{ab} and ϵ^{abc} (for Cartesian indices $a, b, \cdots$). Under the parity transformation, all vectors pick up a factor of -1; this implies that parity-odd correlators *must* contain an odd number of Levi-Cevita symbols, ϵ^{abc}, since there is no other way to combine an odd number of vectors to form a scalar.

In Fourier space, ζ depends on some set of wave vectors, $\mathbf{k}_1, \ldots, \mathbf{k}_n$ (each associated to a single $\mathbf{r}_i$), which transform as follows under parity:

$$\mathbb{P}[\zeta(\mathbf{k}_1, \ldots, \mathbf{k}_n)] = \zeta(-\mathbf{k}_1, \ldots, -\mathbf{k}_n). \tag{2}$$

Often, ζ is the correlation of some number of real fields; in this case, $\zeta(-\mathbf{k}_1, \ldots, -\mathbf{k}_n) = \zeta^*(\mathbf{k}_1, \ldots, \mathbf{k}_n)$; thus parity-even (parity-odd) correlators are purely real (imaginary). Analogously to before, any parity-odd correlator in Fourier-space requires a Levi-Cevita symbol, leading to a term of the form $\mathbf{k}_i \cdot \mathbf{k}_j \times \mathbf{k}_k$ (since k derivatives are killed by locality). Importantly, the scalar triple product is the simplest geometric object that is (a) parity sensitive, (b) isotropic and (c) a scalar. This immediately gives rise to an important conclusion (which we prove below): for scalar observables parity violation can be probed only in the four-point function and above (for three-point functions, e.g., bispectra $B(\mathbf{k}_1, \mathbf{k}_2, \mathbf{k}_3)$, the three vectors sum to zero; thus the triple product is trivial).

B. Correlators: Heuristic argument

Physical symmetries place strong restrictions on the parity sensitivity of various observables. Here, we will consider explicitly the general form of the power spectrum, bispectrum, and trispectrum of real fields, and argue that, in expectation, only the latter is parity sensitive. Our arguments are nonperturbative, and thus apply in arbitrarily nonlinear regimes, though require all observables to be averaged over realizations.

By translation invariance, the two-, three-, and four-point correlators of real fields X, Y, Z, W must satisfy momentum conservation:

$$\begin{aligned}
\langle X(\mathbf{k}_1)Y(\mathbf{k}_2)\rangle &= P_{XY}(\mathbf{k}_1)(2\pi)^3\delta_{\mathrm{D}}(\mathbf{k}_1+\mathbf{k}_2)\\
\langle X(\mathbf{k}_1)Y(\mathbf{k}_2)Z(\mathbf{k}_3)\rangle &= B_{XYZ}(\mathbf{k}_1,\mathbf{k}_2,\mathbf{k}_3)(2\pi)^3\delta_{\mathrm{D}}(\mathbf{k}_1+\mathbf{k}_2+\mathbf{k}_3)\\
\langle X(\mathbf{k}_1)Y(\mathbf{k}_2)Z(\mathbf{k}_3)W(\mathbf{k}_4)\rangle &= T_{XYZW}(\mathbf{k}_1,\mathbf{k}_2,\mathbf{k}_3,\mathbf{k}_4)(2\pi)^3\delta_{\mathrm{D}}(\mathbf{k}_1+\mathbf{k}_2+\mathbf{k}_3+\mathbf{k}_4).
\end{aligned} \tag{3}$$

Asserting rotational invariance (ignoring, e.g., wide-angle effects), each correlator can depend only on scalar functions derived from the $\mathbf{k}_i$ wave numbers, as discussed above. In three dimensions, these comprise only $|\mathbf{k}| \equiv k$, $\mu_{ij} \equiv \hat{\mathbf{k}}_i \cdot \hat{\mathbf{k}}_j$, $\hat{\mathbf{k}}_i \cdot \hat{\mathbf{k}}_j \times \hat{\mathbf{k}}_k$ leading to the definitions

$$\begin{aligned}
P_{XY}(\mathbf{k}_1) &= P_{XY}(k_1)\\
B_{XYZ}(\mathbf{k}_1,\mathbf{k}_2,\mathbf{k}_3) &= B_{XYZ}(k_1,k_2,k_3,\mu_{12},\mu_{13},\mu_{23},\hat{\mathbf{k}}_1\cdot\hat{\mathbf{k}}_2\times\hat{\mathbf{k}}_3) = B_{XYZ}(k_1,k_2,k_3)\\
T_{XYZW}(\mathbf{k}_1,\mathbf{k}_2,\mathbf{k}_3,\mathbf{k}_4) &= T_{XYZW}(k_1,k_2,k_3,k_4,|\mathbf{k}_1+\mathbf{k}_2|,|\mathbf{k}_1+\mathbf{k}_3|,\mu_{12},\mu_{13},\mu_{14},\mu_{23},\mu_{24},\mu_{34},\hat{\mathbf{k}}_1\cdot\hat{\mathbf{k}}_2\times\hat{\mathbf{k}}_3)\\
&= T_{XYZW}(k_1,k_2,k_3,k_4,|\mathbf{k}_1+\mathbf{k}_2|,|\mathbf{k}_1+\mathbf{k}_3|,\hat{\mathbf{k}}_1\cdot\hat{\mathbf{k}}_2\times\hat{\mathbf{k}}_3),
\end{aligned} \tag{4}$$

where we eliminate degenerate variables to reach the second definitions, using conservation of momentum. As above, parity inversion leads to the mapping $\mathbf{k} \to -\mathbf{k}$, and, if the fields are real, a complex conjugation; it is immediately apparent that P_{XY} and B_{XYZ} are invariant under this transformation, and are thus parity insensitive and real. In contrast, the trispectrum (and any higher-order correlators) contains the irreducible triple product $\hat{\mathbf{k}}_1 \cdot \hat{\mathbf{k}}_2 \times \hat{\mathbf{k}}_3$, which allows it to be parity sensitive, and, in general, complex.

C. Correlators: Formal proof

Whilst the above argument suffices to demonstrate that (realization-averaged) power spectra and bispectra cannot probe parity-violating physics, due to their lack of dependence on the scalar triple product, some readers may wish for a more formal argument. To this end, let us assume some primordial source of parity violation, through the gravitational potential ϕ. By the above arguments, this must involve a scalar triple product, taking the heuristic form

$$\phi^{\rm NG}(\mathbf{k}) = \phi^{\rm G}(\mathbf{k}) + ip_{\rm NL}\int_{\mathbf{p}_1+\mathbf{p}_2+\mathbf{p}_3=\mathbf{k}} (\mathbf{p}_1\cdot\mathbf{p}_2\times\mathbf{p}_3) f[\phi^{\rm G}](\mathbf{p}_1,\mathbf{p}_2,\mathbf{p}_3) + \cdots, \tag{5}$$

where $\phi^{\rm G}$ is the Gaussian potential, $\int_{\mathbf{p}} \equiv \int d^3p/(2\pi)^3$, and the scalar functional f will be discussed in Sec. III. Here, the magnitude of parity violation is set by the imaginary parameter $ip_{\rm NL}$. Searching for late-time manifestations of parity violation is thus equivalent to finding realization-averaged observables that depend on $ip_{\rm NL}$. Notably, those depending on *even* powers of $ip_{\rm NL}$ are not signatures of parity violation, since the square of a parity-odd contribution is parity even. For this reason, we will consider simulations with both positive and negative $p_{\rm NL}$ to validate our arguments below, since their difference removes any quadratic (and higher) $ip_{\rm NL}$ contributions.

Any late-time field $X(\mathbf{k})$ is uniquely determined by the primordial potential $\phi^{\rm NG}$, and can thus be written as a formal Taylor series:

$$X(\mathbf{k}) = \sum_{n=0}^{\infty}\int_{\sum_i \mathbf{q}_i=\mathbf{k}} X^{(n)}(\mathbf{q}_1,\ldots,\mathbf{q}_n;\mathbf{k})\phi^{\rm NG}(\mathbf{q}_1)\cdots\phi^{\rm NG}(\mathbf{q}_n), \tag{6}$$

where the nth order piece involves n primordial potentials. The deterministic kernel $X^{(n)}$ is fixed by the equations of motion (independently of inflationary physics); ignoring late-time parity violation, it can depend only on magnitudes $|\mathbf{q}_i|$ and angles $\hat{\mathbf{q}}_i\cdot\hat{\mathbf{q}}_j$.[2] Expanding the potentials to first order in $ip_{\rm NL}$ leads to the formal contribution to the power spectrum (which remains nonperturbative and could include arbitrary nonlinearity, loops, counterterms, and beyond):

$$P_{XY}(\mathbf{k}) \supset \sum_{n=1}^{\infty}\int_{\sum_i \mathbf{q}_i=\mathbf{k}} [ip_{\rm NL}(\mathbf{q}_1\cdot\mathbf{q}_2\times\mathbf{q}_3)]\times K^{(n)}_{XY}(q_i,k,\hat{\mathbf{k}}\cdot\hat{\mathbf{q}},\hat{\mathbf{q}}_i\cdot\hat{\mathbf{q}}_j)\times[P_\phi(q_i)P_\phi(|\mathbf{k}-\mathbf{q}_i|)\cdots], \tag{7}$$

where $K^{(n)}_{XY}$ is the nth order kernel which is built from $X^{(n)}$ and $Y^{(n')}$ and P_ϕ is the power spectrum of $\phi^{\rm NG}$. Here, the parity-violating initial conditions source the square bracket, including both $ip_{\rm NL}$ and a scalar triple product. Under the transformation $\mathbf{k}\to-\mathbf{k}$ and a relabeling $\mathbf{q}_i\to-\mathbf{q}_i$, we find $P^{(ip_{\rm NL})}_{XY}(-\mathbf{k}) = -P^{(ip_{\rm NL})}_{XY}(\mathbf{k})$, since $K^{(n)}_{XY}$ depends only on magnitudes and angles so is invariant, yet $\mathbf{q}_1\cdot\mathbf{q}_2\times\mathbf{q}_3$ changes sign. Since rotational invariance restricts us to power spectra of the form $P_{XY}(\mathbf{k}) = P_{XY}(k)$, this implies that the order $ip_{\rm NL}$ contribution must vanish. An analogous argument implies that higher odd powers of $ip_{\rm NL}$ vanish; thus the overall power spectrum is parity insensitive. By a similar line of reasoning, the bispectrum must also be parity even; however, the trispectrum can exhibit signatures of parity violation, since rotational symmetry does not demand it to be independent of $\hat{\mathbf{k}}$.

Before continuing, we briefly remark on violations of the above assumptions. The most pertinent of these is the breaking of rotational invariance through redshift-space distortions. In this case, the problem contains an additional vector: the (assumed global) line of sight $\hat{\mathbf{n}}$. For the power spectrum, symmetry then dictates $P_{XY}(\mathbf{k}_1) = P_{XY}(k_1,\hat{\mathbf{k}}_1\cdot\hat{\mathbf{n}})$. Note that as exchanging $X\leftrightarrow Y$ is equivalent to $\mathbf{k}_1\to-\mathbf{k}_1$, a signature of parity violation can occur only for cross spectra with $X\neq Y$ [as $P_{XX}(\mathbf{k})-P_{XX}(-\mathbf{k})=0$ by definition]. Furthermore, parity violation is equivalent to replacing the line of sight $\hat{\mathbf{n}}$ with $-\hat{\mathbf{n}}$: however, this is an isometry of the equations of motion; thus there again can be no signal proportional to $ip_{\rm NL}$. To see this, note the formal expansion for the redshift-space power spectrum:

[2] If there were late-time parity violation, the $X^{(n)}$ kernels would include a parity-odd triple product of the form $(i\sigma)\mathbf{q}_1\cdot\mathbf{q}_2\times\mathbf{q}_3$, for amplitude parameter $i\sigma$. The coupling of this to the $ip_{\rm NL}$ triple product in the initial conditions would source *parity-even* physics linear in $ip_{\rm NL}$ (via $i^2p_{\rm NL}\sigma$). However, since the underlying equations of gravitation and hydrodynamics are parity even, this cannot be sourced by standard physics at any order.

$$P_{XY}(k,\hat{\mathbf{k}}\cdot\hat{\mathbf{n}}) \supset \sum_{n=1}^{\infty}\int_{\sum_i \mathbf{q}_i=\mathbf{k}} [ip_{\rm NL}(\mathbf{q}_1\cdot\mathbf{q}_2\times\mathbf{q}_3)]\times K_{XY}^{(n)}(q_i,k,\hat{\mathbf{k}}\cdot\hat{\mathbf{q}},\hat{\mathbf{q}}_i\cdot\hat{\mathbf{q}}_j,\hat{\mathbf{q}}_i\cdot\hat{\mathbf{n}},\hat{\mathbf{k}}\cdot\hat{\mathbf{n}})[P_\phi(q_i)P_\phi(|\mathbf{k}-\mathbf{q}_i|)\cdots]. \tag{8}$$

Here the line of sight $\hat{\mathbf{n}}$ enters only in the kernels (since it impacts the transformation between observables and initial conditions). Importantly, these kernels are invariant under $\hat{\mathbf{n}}\to-\hat{\mathbf{n}}$ due to cylindrical symmetry (i.e. the fact that the line of sight is defined only up to 180° rotations).[3] Since $\hat{\mathbf{n}}$ does not couple to the initial conditions, we find that, under $\mathbf{k}\to-\mathbf{k}$, $\hat{\mathbf{n}}\to-\hat{\mathbf{n}}$ and relabeling $\mathbf{q}\to-\mathbf{q}$, $P_{XY}^{(ip_{\rm NL})}(k,\hat{\mathbf{k}}\cdot\hat{\mathbf{n}})$ transforms to $-P_{XY}^{(ip_{\rm NL})}(k,\hat{\mathbf{k}}\cdot\hat{\mathbf{n}})$; thus the contribution must vanish. The same logic applies to the bispectrum, whence parity violation is equivalent to $\hat{\mathbf{n}}\to-\hat{\mathbf{n}}$ as before, but the kernels remain invariant under $\hat{\mathbf{n}}\to-\hat{\mathbf{n}}$.

D. Halo mass function

Next, we consider the halo mass function, $n(M)$. Once again, this is not parity sensitive. Formally, an explicit expression for $n(M)$ is given by as a Taylor series in Fourier space (cf. (6):

$$\hat{n}(M) = \sum_{n=0}^{\infty}\int_{\sum_i \mathbf{q}_i=\mathbf{0}} N^{(n)}(\mathbf{q}_1,\ldots,\mathbf{q}_n,M)\phi^{\rm NG}(\mathbf{q}_1)\cdots\phi^{\rm NG}(\mathbf{q}_n), \tag{9}$$

for some kernel $N^{(n)}$. Averaging over the initial conditions, we find the following schematic contribution at first order in $ip_{\rm NL}$:

$$n(M) \supset \sum_{n=1}^{\infty}\int_{\sum_i \mathbf{q}_i=\mathbf{0}} [ip_{\rm NL}(\mathbf{q}_1\cdot\mathbf{q}_2\times\mathbf{q}_3)]\times \overline{N}^{(n)}(q_i,\hat{\mathbf{q}}_i\cdot\hat{\mathbf{q}}_j,M)\times[P_\phi(q_1)\cdots], \tag{10}$$

with new kernel $\bar{N}^{(n)}$. Under the relabeling $\mathbf{q}\to-\mathbf{q}$, we find $n^{(ip_{\rm NL})}(M) = -n^{(ip_{\rm NL})}(M)$; thus the contribution is zero. The same holds at higher (odd) orders.

E. Halo angular momenta

In the above discussion, we have considered only scalar observables, such as the matter density or mass function. Different behavior can arise if one instead works with tensor observables, since these carry additional directional information, bypassing the above symmetry constraints. For the CMB, the principal example is polarization, which allows for parity-sensitive two-point correlators (TB and EB spectra) [6,7,9–11,13,31–35]. In the context of the late Universe, the simplest tensor fields at our disposal are the shapes of galaxies, as well as the velocity and angular momentum fields of tracer particles, such as halos or galaxies. The former are difficult to probe using N-body simulations; thus we will restrict our attention to the latter in this work.

Under a parity transform, velocity transforms as a vector (with $\mathbb{P}[\mathbf{v}(\mathbf{r})] = -\mathbf{v}(-\mathbf{r})$), whilst the angular momentum transforms as an axial vector (with $\mathbb{P}[\mathbf{J}(\mathbf{r})] = \mathbf{J}(-\mathbf{r})$). As such, the combination $\mathbf{J}\cdot\mathbf{v}$ is a pseudoscalar, which changes sign under point reflections. This enables a convenient test: averaging over a sufficiently large number of objects, the cosine $\hat{\mathbf{J}}\cdot\hat{\mathbf{v}}$ can take nonzero values only if parity symmetry is broken. In the above language, $\hat{\mathbf{J}}\cdot\hat{\mathbf{v}}$ must be proportional to odd powers of the parity-breaking amplitude $ip_{\rm NL}$. We will use this notion to probe parity violation in Sec. V.

Furthermore, one can decompose (axial) vectors such as the angular momentum into left- and right-handed components, and thus evaluate their chirality. This was demonstrated in [29] (and later works [28,36–38]), considering the quantity $\mu_{L,R}\equiv\hat{\mathbf{J}}\cdot\hat{\mathbf{J}}_{L,R}$, where $\hat{\mathbf{J}}$ is the observed halo angular momentum, and $\hat{\mathbf{J}}_{L,R}$ is a proxy constructed from the primordial density field. From the sum $\mu_L+\mu_R$, one can probe if galaxy angular momentum is correlated with the initial conditions; from the difference, one can probe parity-violating processes. This will again be explored in Sec. V.

F. Summary

The conclusion of the above discussion is that the parity violation is difficult to observe when considering only scalar observables, such as the mass and halo density fields.

[3]This can be violated with wide-angle effects, since there are then two distinct lines of sight. Such an effect cannot be probed with standard N-body simulations however.

At arbitrarily nonlinear scales, the power spectrum, bispectrum, and halo mass function are unaffected by parity violation injected in the initial conditions, i.e. they are independent of the sign of $p_{\rm NL}$. As such, suites of simulations with $+|p_{\rm NL}|$ and $-|p_{\rm NL}|$ should yield the same averaged statistics in arbitrarily nonlinear regimes, a prediction that we verify in Sec. V. To probe parity violation with scalar observables, we require quantities which depend on *at least three* independent vector coordinates (e.g., $\mathbf{k}_1$, $\mathbf{k}_2$, $\mathbf{k}_3$, needed to form a scalar triple product), the simplest of which is the parity-odd trispectrum. Importantly, parity-odd statistics such as this cannot be sourced by canonical gravitational or hydrodynamic physics (which is parity odd); any detection would thus indicate strong evidence for new physics.

In contrast, tensorial observables can probe parity violation with simpler statistics. A particularly notable example is the angular momentum of tracers, which probes the mirror asymmetries both via its helicity decomposition, and its scalar product with the velocity field (and cannot be sourced by conventional physics).[4] Such quantities may have limitations in practice however, since we have access only to projected velocity fields, and can measure only the tangential angular momentum, through galaxy spin [e.g. [36]]. Though beyond the scope of this work, EB galaxy shear correlations may also be an intriguing probe of parity violation.

III. PARITY VIOLATION IN PRACTICE: INITIAL CONDITIONS

A. Definition

We now consider how to create simulations with injected parity violation. Analogously to the case of three-point non-Gaussianities (proportional to $f_{\rm NL}$) [39], our procedure is to first generate a Gaussian primordial potential, $\phi^{(1)}(\mathbf{x})$, and then modulate it to source the correlators of interest. Definitively, we perform the following transformation:

$$\phi^{\rm NG}(\mathbf{x}) = \phi^{(1)}(\mathbf{x}) \to \phi^{(1)}(\mathbf{x}) + p_{\rm NL}[\epsilon^{ijk}(\partial_i|\partial|^\alpha\phi^{(1)})(\partial_j|\partial|^\beta\phi^{(1)})(\partial_k|\partial|^\gamma\phi^{(1)})](\mathbf{x}), \tag{11}$$

where $\alpha \neq \beta \neq \gamma$ are integers, $p_{\rm NL}A_s$ controls the amplitude of parity violation (for inflationary amplitude A_s), and $|\partial|^\alpha$ corresponds to a Fourier-space multiplication by k^α. As discussed in Sec. II, this is parity violating due to the presence of a Levi-Cevita symbol, which must be contracted with three different fields. If the initial conditions are to be scale invariant, we require a trispectrum scaling as $(P_\phi)^3$: this is achieved by setting $\alpha+\beta+\gamma=-3$.[5] Below, we will set $\{\alpha,\beta,\gamma\} = \{-2,-1,0\}$. Notably, (11) does not represent all possible parity-violating initial conditions, much as the local bispectrum shape does not represent all types of three-point primordial non-Gaussianity (PNG). Different models of new physics generate distinct primordial signatures which can be more complex than the above; the only generic prediction is that the modification to the potential must contain an odd number of Levi-Cevita symbols (to ensure parity-violation).

Defining the Fourier-space field by $\phi(\mathbf{k}) \equiv \int d\mathbf{x}\, e^{-i\mathbf{k}\cdot\mathbf{x}}\phi(\mathbf{x})$, the correction term in (11) can be written:

$$\phi^{(3)}(\mathbf{k}) = ip_{\rm NL}\int_{\mathbf{p}_1\mathbf{p}_2\mathbf{p}_3}(2\pi)^3\delta_{\rm D}(\mathbf{k}-\mathbf{p}_1-\mathbf{p}_2-\mathbf{p}_3)[\mathbf{p}_1\cdot\mathbf{p}_2\times\mathbf{p}_3]p_1^\alpha p_2^\beta p_3^\gamma\phi^{(1)}(\mathbf{p}_1)\phi^{(1)}(\mathbf{p}_2)\phi^{(1)}(\mathbf{p}_3), \tag{12}$$

as in (5). Practically, this is easiest to compute as a summation in real space, having first computed the gradient fields $\partial_i|\partial|^\alpha\phi^{(1)}$ via Fourier transforms. We stress that such simplifications are possible only due to our assumption of a separable form for the primordial parity-odd distortion.

The above modification to the primordial potential generically leads to corrections to the power spectrum at $\mathcal{O}(p_{\rm NL}^2)$, which become relevant on small scales.[6] These may be optionally removed by rescaling the non-Gaussian initial conditions via

[4]It is interesting to consider whether the angular momentum field can impart parity sensitivity on power spectra (and beyond) via observational selection effects, such as $\delta \propto \hat{\mathbf{n}}\cdot\hat{\mathbf{J}}$ (i.e. a tendency to observe more face-on than edge-on galaxies). Since the statistics of the angular momentum field are themselves isotropic and there is only one global axis in the problem ($\hat{\mathbf{n}}$), any contractions with the Levi-Cevita symbol must vanish; thus such phenomena cannot affect matter correlators.

[5]This can also be implemented by acting on the above with $|\partial|^{-\alpha-\beta-\gamma-3}$.

[6]As discussed in Sec. II, rotation and translation invariance forbids any $\mathcal{O}(p_{\rm NL})$ corrections from appearing. Since the residual corrections do not depend on the sign of $p_{\rm NL}$, they are not parity sensitive.

$$\phi^{\rm NG}(\mathbf{k}) \to \sqrt{\frac{\langle\phi^{(1)}(\mathbf{k})\phi^{(1)*}(\mathbf{k})\rangle}{\langle\phi^{\rm NG}(\mathbf{k})\phi^{\rm NG*}(\mathbf{k})\rangle}}\phi^{\rm NG}(\mathbf{k}), \tag{13}$$

which ensures that the output power spectrum is invariant, upon averaging over realizations. Since this factor is $1+\mathcal{O}(p_{\rm NL}^2)$, we will ignore it in computation of the theoretical parity-odd trispectrum below.

B. Correlators

Our ansatz for the primordial potential of (12) generates a parity-violating trispectrum that is the sum of four components, each of the form

$$\begin{aligned} T^{1113}(\mathbf{k}_1,\mathbf{k}_2,\mathbf{k}_3,\mathbf{k}_4) &= \langle\delta^{(1)}(\mathbf{k}_1)\delta^{(1)}(\mathbf{k}_2)\delta^{(1)}(\mathbf{k}_3)\delta^{(3)}(\mathbf{k}_4)\rangle \\ &= -ip_{\rm NL}[\mathbf{k}_1\cdot\mathbf{k}_2\times\mathbf{k}_3]P_\phi(k_1)P_\phi(k_2)P_\phi(k_3)\{k_1^\alpha k_2^\beta k_3^\gamma - k_1^\alpha k_2^\gamma k_3^\beta + (4\text{ perms.})\}, \end{aligned} \tag{14}$$

summing over a total of six permutations. The full trispectrum becomes

$$T_\phi(\mathbf{k}_1,\mathbf{k}_2,\mathbf{k}_3,\mathbf{k}_4) = -ip_{\rm NL}[\mathbf{k}_1\cdot\mathbf{k}_2\times\mathbf{k}_3]P_\phi(k_1)P_\phi(k_2)P_\phi(k_3)k_1^\alpha k_2^\beta k_3^\gamma + 23\text{ perms.} + \mathcal{O}(p_{\rm NL}^2), \tag{15}$$

where odd permutations of $\{\mathbf{k}_1,\mathbf{k}_2,\mathbf{k}_3,\mathbf{k}_4\}$ pick up a negative sign due to the cross product. As discussed in Sec. II, this is odd under the exchange of $\mathbf{k}\to-\mathbf{k}$ (which leads to parity violation) and purely imaginary. Whilst this polynomial form is not the most general parity-odd trispectrum considered, it is likely that other physical models of parity violation (such as those considered in [20,23,24]), can be projected onto templates such as the above, and thus efficiently constrained (analogous to the use of equilateral, orthogonal, and local shapes in bispectrum studies).

It is further instructive to consider the other primordial correlators. First, there is strictly a parity-even contribution to the trispectrum: this appears only one-loop however, requiring diagrams of the form T^{3311}, which are suppressed by a factor of $p_{\rm NL}A_s$. In contrast, the primordial bispectrum is zero at all orders in $p_{\rm NL}A_s$; this occurs since $\phi^{\rm NG}$ contains only pieces linear and cubic in $\phi^{(1)}$; thus all Wick contractions contain an odd number of fields, and hence evaluate to zero. Finally, we note that the power spectrum naïvely contains a parity-sensitive 13-diagram, but this is equal to zero:

$$\begin{aligned} P^{13}(\mathbf{k}) &= ip_{\rm NL}k^\alpha P_\phi(k)\int_{\mathbf{p}}[\mathbf{k}\cdot\mathbf{p}\times-\mathbf{p}]p^{\beta+\gamma}P_\phi(p) \\ &\quad + 2\text{ perms.} = 0. \end{aligned} \tag{16}$$

At two-loop order, there exists a 33-diagram, given by

$$\begin{aligned} P^{33}(\mathbf{k}) = p_{\rm NL}^2\int_{\mathbf{p}_1\mathbf{p}_2\mathbf{p}_3}&(2\pi)^3\delta_{\rm D}(\mathbf{k}-\mathbf{p}_1-\mathbf{p}_2-\mathbf{p}_3)[\mathbf{p}_1\cdot\mathbf{p}_2\times\mathbf{p}_3]^2P_\phi(p_1)P_\phi(p_2)P_\phi(p_3) \\ &\times p_1^\alpha p_2^\beta p_3^\gamma\{p_1^\alpha p_2^\beta p_3^\gamma + p_1^\beta p_2^\gamma p_3^\alpha + p_1^\gamma p_2^\alpha p_3^\beta - p_1^\alpha p_2^\gamma p_3^\beta - p_1^\beta p_2^\alpha p_3^\gamma - p_1^\gamma p_2^\beta p_3^\alpha\}. \end{aligned} \tag{17}$$

This is generically suppressed by $(p_{\rm NL}A_s)^2$ compared to the tree-level P_ϕ prediction. One can show that the contribution scales as k^2 in the infrared ($k\to0$) and, at most, as $k^{2\,\max\{\alpha,\beta,\gamma\}+2}P_\phi(k)$ in the ultraviolet ($k\to\infty$); thus our modification to the initial conditions is well defined.[7] In practice, this contribution is removed via the rescaling of (13).

C. Validation

To validate the initial condition generation procedure we generate 1000 simulations of the primordial potential: 500 with $p_{\rm NL}=+10^6$ and 500 with $p_{\rm NL}=-10^6$. We then performed a range of tests including verifying that our rescaling, (13), removes the majority of the $\mathcal{O}(p_{\rm NL}^2)$ power spectrum contribution and verifying that we did not generate a spurious primordial bispectrum. A key test is to examine the primordial trispectrum, and compare its

[7]This differs from [39], who find large divergences in P_{22} for some forms of initial condition generation. The difference here is that, due to the imposed condition $\alpha+\beta+\gamma=-3$, we do not have derivative operators acting on the entire $\phi^{(3)}$, which would yield reciprocal powers of k in the infrared limit.

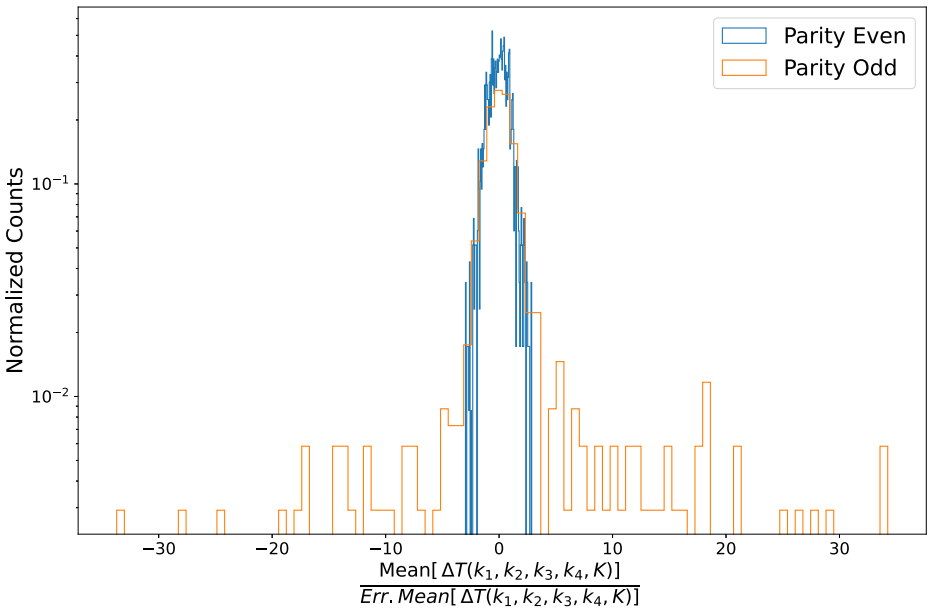

FIG. 2. As a validation of the parity-violating initial conditions, we measure the binned parity-even and parity-odd trispectrum signals from the primordial potential, canceling sample variance by computing the difference between this measurement and a Gaussian simulation with matched phases (here and hereafter denoted ΔT). Here, we compare the mean trispectrum to the error on the mean, on a bin-by-bin basis (using 500 simulations of each type). It can be seen that the parity-even results are consistent with the noise distribution shown in black (as expected, since the signal appears only at second order), but there is clear evidence of a leading-order parity-odd trispectrum.

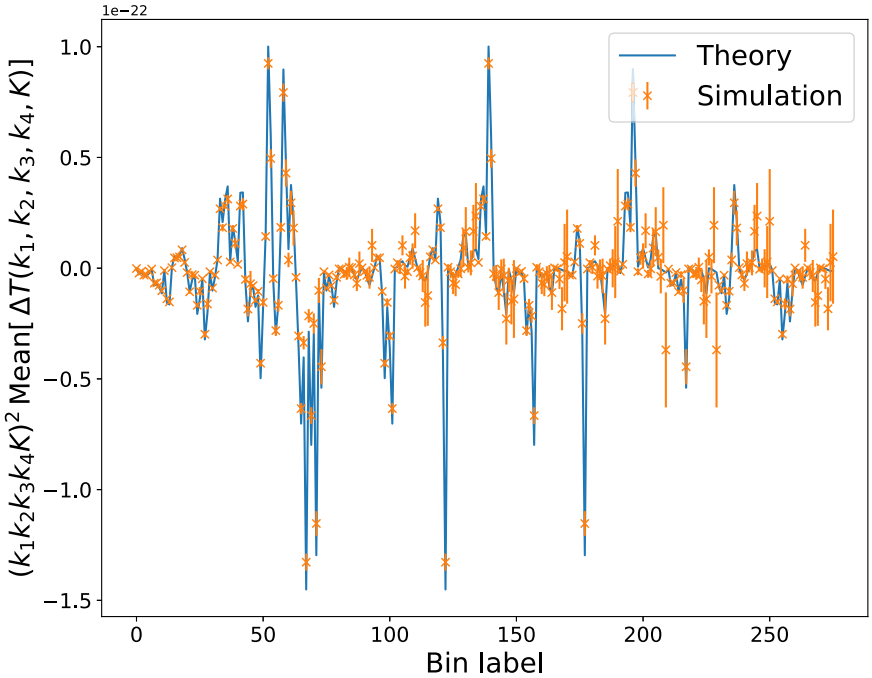

FIG. 3. A comparison of the theoretical and simulated parity-odd trispectrum signals. To reduce noise we compute the difference in the trispectra (ΔT) between simulations with $p_{\rm NL} = 10^6$ and Gaussian simulations with an identical random seed. Theoretical predictions are obtained as in Appendix B (for the input value $p_{\rm NL} = 10^6$), discretizing each bin into a number of sub-bins and averaging the corresponding trispectra (which is not an exact solution, but approximately correct). The high level of agreement provides a stringent test that our initial condition generation produces the correct signal with the relevant value of $p_{\rm NL}$.

TABLE I. Simulation parameters for the QUIJOTE-ODD suite. These use the same parameters as the QUIJOTE and QUIJOTE-PNG simulations [40,41], but feature nonzero parity-violation parameters $p_{\rm NL}$. In each case, the initial conditions are generated with a suitably modified version of the 2LPTIC code [39].

Type	Ω_m	Ω_Λ	Ω_b	σ_8	h	n_s	$\sum m_\nu$ (eV)	w	$L_{\rm box}$ (Mpc/h)	$N^{\frac{1}{3}}_{\rm particles}$	Realizations	$p_{\rm NL}$	$M_{\rm min}$ ($M_\odot/h$)
Parity+	0.3175	0.6825	0.049	0.834	0.6711	0.9624	0.0	−1	1000	512	500	$+10^6$	6.56×10^{11}
Parity−	0.3175	0.6825	0.049	0.834	0.6711	0.9624	0.0	−1	1000	512	500	-10^6	6.56×10^{11}

amplitude to the above theory model. Thus we applied estimators for the binned parity-even and parity-odd trispectrum, described in detail in Appendix A, to test that we did not generate a parity-even trispectrum and that we generated the correct parity-odd signal. For both estimators we used six bins linearly spaced with bin centers spaced between $k = 0.02h$ Mpc^{-1} and $k = 0.12h$ Mpc^{-1}.

In Fig. 2 we show the significance of the detection of the parity-even and parity-odd trispectra. We find no evidence for a parity-even trispectrum, which matches expectations, since this signal should appear only at $\mathcal{O}(p^2_{\rm NL})$. In contrast, there is strong evidence for a parity-odd trispectrum. To validate that the correct parity-odd trispectrum signal is generated, we compare the measured trispectrum to the theoretical expectation—the computation of the expected binned signal is given in Appendix B 2. As can be seen in Fig. 3, the theoretical trispectrum and measured trispectrum show great agreement across a range of scales and tetrahedron configurations for our input value of $p_{\rm NL}$.[8]

IV. PARITY VIOLATION IN PRACTICE: SIMULATIONS

Armed with the parity-violating initial conditions, we now proceed to run the forward model, i.e. to generate parity-violating N-body simulations. These are generated in an identical manner to the QUIJOTE simulations [40,41]. We provide a brief summary of the suite below and refer the reader to [40] and [42] for more details. Table I summarizes the key simulation parameters used in this work.

First a realization of the primordial potential is generated on a 1024^3 grid, and the parity-violating trispectrum is added, via (11). In this work we generate simulations with $p_{\rm NL} = \pm10^6$. These values were chosen as the size of the induced trispectrum is large enough to generate measurable signals, but small enough such that the higher order corrections ($\sim\mathcal{O}(p^2_{\rm NL})$) are still small. We ran a small number of simulations with different $p_{\rm NL}$ values to validate this choice. Next, we perform a rescaling of the initial conditions to mitigate the impact of the $p^2_{\rm NL}$ terms using (13). The initial conditions are then evolved to $z = 0$ using a transfer function computed by CAMB [43] and then rescaled back to $z = 127$ using a scale-independent growth factor. The density field at $z = 127$ is then combined with 2LPT to compute particle displacements and peculiar velocities for glass-distributed particles.

The particles are then evolved using GADGET-3, a treePM code [44]. In total we run 1,000 simulations: 500 with $p_{\rm NL} = +10^6$ and 500 with $p_{\rm NL} = -10^6$. All simulations contain 512^3 particles in a comoving periodic box of $(1000h^{-1}\ {\rm Mpc})^3$. The value of the parameters used to control the accuracy and precision of the different integrators are identical to those used for the QUIJOTE simulations [40]. Halos are identified using both the Friends-of-Friends (FoF) algorithm [45] and ROCKSTAR [46]. We note that while FoF halo catalogs only include positions, masses, and velocities, the Rockstar catalogs include a much richer set of properties such as angular momentum and radius, which will be of great use in Sec. V. Finally, we create overdensity grids from the output particle positions and halo catalogs. This uses the "Cloud-in-Cell" grid assignment scheme [47] to produce grids of size 512^3.

V. PARITY VIOLATION IN PRACTICE: LATE-TIME OBSERVABLES

In this section we explore a range of commonly considered statistical probes and examine how they are changed by the presence of the parity-violating primordial trispectrum. Here, our focus is on the $z = 0$ universe; similar results were found at $z = 1$. Furthermore, to isolate the terms linear in $p_{\rm NL}$ and remove any $p^2_{\rm NL}$ terms, which are not parity violating, we show most of the results as the difference between the $p_{\rm NL} = 10^6$ and $p_{\rm NL} = -10^6$ simulations.

A. Power spectrum

We compute the power spectrum of the halo and matter field using PYLIANS [48], in a similar manner to [41,49]. In Fig. 4 we show the impact of the parity violation PNG on the power spectrum: averaging over realizations, there is seen to be no effect in either the matter or halo power spectrum. Note that the matter power spectrum shows a small dip at small scales, and similar effects were seen in the initial conditions. This is not thought to be a signature of $p_{\rm NL}$ in the power spectrum. This deviation arises as the quadratic (parity-even) terms in $p_{\rm NL}$ lead to strong correlations between $P(k)$ and $P(k')$ and an increase in the small

[8]We have further verified that our parity-odd estimator is unbiased by computing the null $\chi^2 \equiv T^2_{\rm odd}/\sigma^2(T_{\rm odd})$ for Gaussian simulations (without cosmic variance cancellation), and verifying that it is consistent with the expected value, $N_{\rm bins}$, to $\approx1\%$.

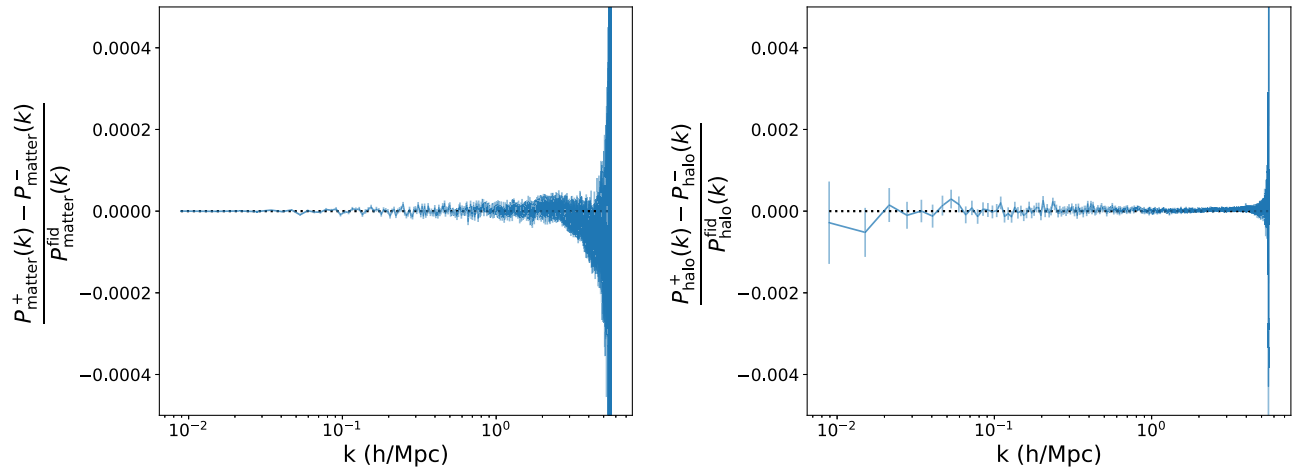

FIG. 4. The response of the $z = 0$ matter power spectrum, left panel, and the halo power spectrum, right panel, to parity-violating non-Gaussianity. This is computed as the difference between 500 simulations with $p_{\rm NL} = 10^6$ and $p_{\rm NL} = -10^6$. The halo power spectrum uses all halos with $M \geq 3.2 \times 10^{13} M_\odot/h$. At leading order in $p_{\rm NL}$ both statistics are unchanged. The error bars on both plots denote the error on the mean, as measured with the 500 simulations.

scale power spectrum variance. This effect will thus average down with a very large number of simulations. In smaller ensembles, this can give rise to features that appear significant as many highly correlated bins can deviate from zero. In our case, the deviation of any single bin is $\sim 1\sigma$ (in the mean), and an examination of the correlation matrix shows these bins are strongly correlated.

B. Matter probability density function and the halo mass function

In Fig. 5 we explore how the matter PDF and HMF are affected. The PDF is computed from the matter density grids, as discussed in Sec. IV, whilst the halo mass function is computed from the FoF halo catalogs as in [50]. As can be seen, we find no detectable average signal of $p_{\rm NL}$ in either statistic. This agrees with the conclusions of Sec. II.

C. Bispectrum

Next, we compute the binned bispectrum in a similar manner to [41,49,51], using 10 bins linearly spaced between $k = 0.013h$ Mpc^{-1} and $k = 0.19h$ Mpc^{-1}. In the left panel of Fig. 6, we show the ratio of the difference in bispectrum bin value between 500 $p_{\rm NL} = 10^6$ and $p_{\rm NL} = -10^6$ simulations to the error on the mean of that bin. Once again, we find no evidence of an induced bispectrum.

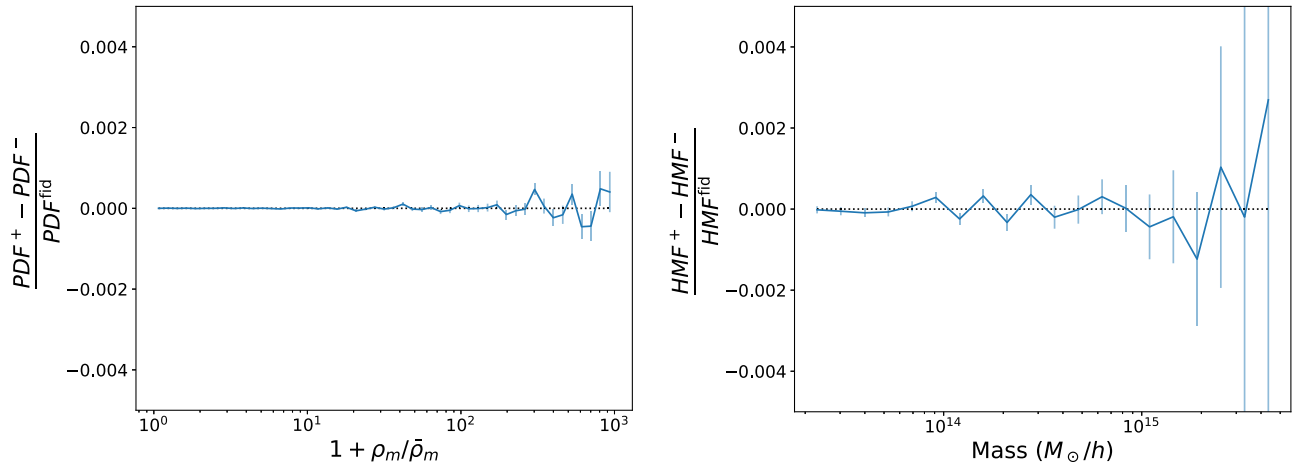

FIG. 5. The response of the $z = 0$ probability density function (PDF, left panel) and the halo mass function (HMF, right panel, computed using the difference of 500 simulations with $p_{\rm NL} = 10^6$ and $p_{\rm NL} = -10^6$. Despite the presence of a large level of primordial non-Gaussianity, both statistics are unaffected. The error bars are the error on the mean. Note that we consider the PDF of $1 + \rho/\bar{\rho}$, where $\bar{\rho}$ is the mean density, to allow the logarithmic axis.

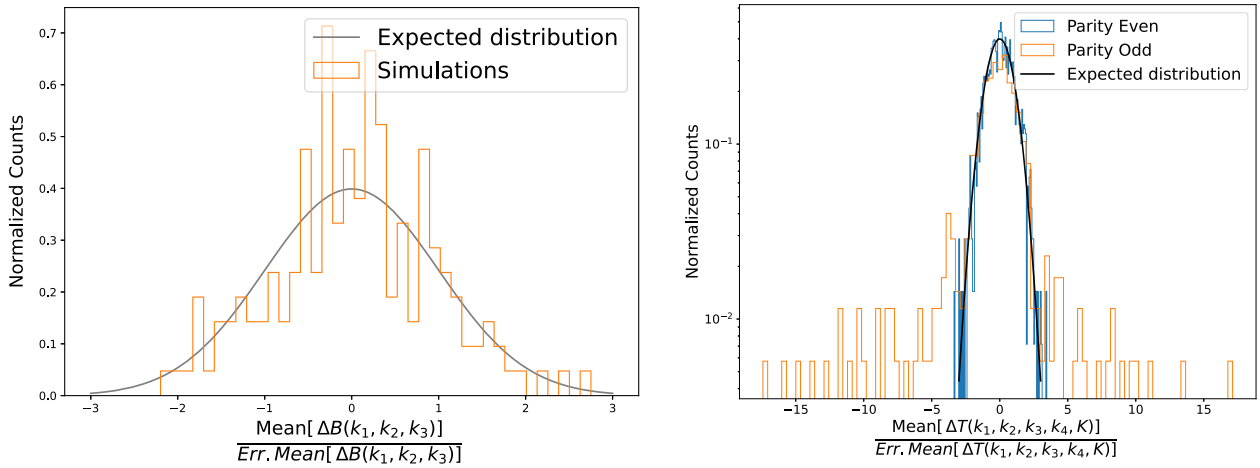

FIG. 6. The impact of the parity-violating trispectrum on the $z = 0$ matter bispectrum (left panel) and the parity-even and parity-odd matter trispectrum (right panel) normalized by the standard error on the mean for each bispectrum/trispectrum bin. As the distribution of bispectrum measurements is consistent with no signal (the blue line), we can conclude that no detectable bispectrum is sourced. The parity-even trispectrum shows a similar result—no signal is detectable, and we match the expected noise distribution shown in black. However, we find strong evidence for a parity-odd trispectrum, implying that this quantity is preserved through cosmic time (though its amplitude is modulated by nonlinear effects). Note that as we show the distribution of the difference between the $p_{\rm NL} = 10^6$ and $p_{\rm NL} = -10^6$ simulations (denoted ΔT), we cancel most of the cosmic variance.

D. Trispectrum

Using the estimators in Appendix A, we measure the parity-even and parity-odd trispectrum with the same binning scheme as for the primordial trispectrum in Sec. III C. As shown in Fig. 6, the parity-even trispectrum measurements are consistent with no induced trispectrum signal, as expected. In contrast, the parity-odd trispectrum shows strong evidence of a signal, though, as expected, none is present if $p_{\rm NL} = 0$. Note that this is computed from the difference of simulations with $p_{\rm NL} = 10^6$ and $p_{\rm NL} = -10^6$, which cancels most of the cosmic variance. Without this technique, the signal-to-noise on the parity-odd signal would be dramatically reduced. In its presence, we find a combined detection significance of around 40σ for a single simulation.[9] Whilst this scales linearly with $p_{\rm NL}$, we caution that the value considered in this work would be essentially impossible to detect from a single 1 $h^{-3}\,{\rm Gpc}^3$ simulation volume if one does not perform cosmic variance cancellation.

E. Halo angular momenta

As discussed in Sec. II E, the angular momenta of simulated tracers can be parity sensitive. Here, we consider two associated tests: (a) correlating halo angular momentum, $\mathbf{J}$, with the velocity field, and (b) correlating halo angular momentum with a chiral proxy derived from the initial conditions. In each case, we use the angular momenta measured from the ROCKSTAR code [52], dropping any subhalos, and considering a minimum mass cut of $3 \times 10^{13} h^{-1} M_\odot$.

In the first case, we compute the velocity field, $\mathbf{v}_R(\mathbf{r})$, from the $z = 127$ snapshot [as $\mathbf{v}(\mathbf{k}, z) = (-i\mathbf{k}/k^2) f(z) \mathcal{H}(z) \times \delta(\mathbf{k}, z)$ for growth rate $f(z)$ and conformal Hubble parameter $\mathcal{H}(z)$], smoothing on a scale $R \in \{2, 5, 10\} h^{-1}$ Mpc. The resulting field is interpolated to the halo positions, and then the cosine $\hat{\mathbf{J}} \cdot \hat{\mathbf{v}}_R$ is computed for each halo in the dataset (dropping the moduli of $\mathbf{J}$ and $\mathbf{v}_R$, since they are scalar quantities, and thus parity insensitive). Figure 7 shows the resulting distribution of $\hat{\mathbf{J}} \cdot \hat{\mathbf{v}}_R$ at redshift zero, averaged over 500 simulations with $p_{\rm NL} \in \{0, \pm 10^6\}$. We find a distinctly nonuniform distribution for small smoothing scales (close to the Lagrangian radii of low mass halos), indicating that halo angular momenta correlate with the primordial density field. The Gaussian PDF appears symmetric (indicating no detectable signal for parity-conserving universes, as expected); when $p_{\rm NL}$ is nonzero, we see asymmetries, which are characteristic signatures of parity violation. This is clearly seen in the binned $\hat{\mathbf{J}} \cdot \hat{\mathbf{v}}_R$ statistic, which is expected to be (statistically) zero in the absence of parity violation. For $M \lesssim 3 \times 10^{14} h^{-1} M_\odot$, we find a highly significant signal for $p_{\rm NL} = \pm 10^6$, indicating that the angular-momentum-velocity cosine is a good probe of parity violation, matching the conclusion of Sec. II.

An alternative approach is to construct the $\hat{\mathbf{J}} \cdot \hat{\mathbf{v}}$ statistic from halo velocities measured by ROCKSTAR, removing the need for the initial conditions.[10] The results for this

[9] This is parametrized by $\sum \overline{\Delta T}^2 / \sigma^2(\Delta T) - N_{\rm bins}$, for parity-odd trispectrum $\Delta T \equiv T(p_{\rm NL} = 10^6) - T(p_{\rm NL} = -10^6)$ in a total of $N_{\rm bins}$ (assumed independent) bins.

[10] An alternative approach is to perform some flavor of reconstruction to obtain the velocity field, such as via baryon acoustic oscillations reconstruction techniques (using the continuity equation) or fully Bayesian methods [cf., [36]].

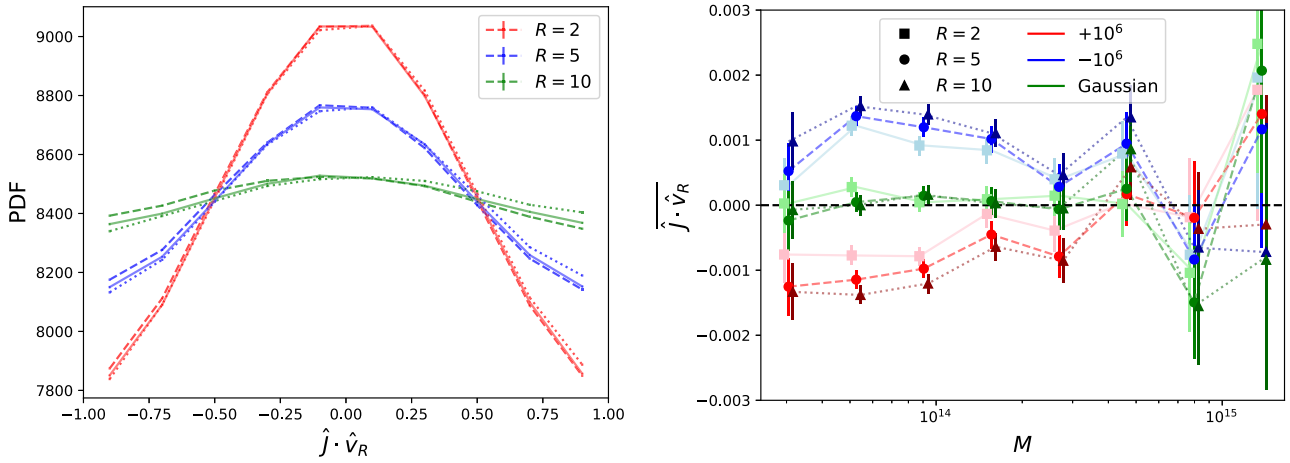

FIG. 7. Correlation between redshift zero halo angular momentum, $\mathbf{J}$, and the velocity field, $\mathbf{v}_R$, measured from the initial conditions, smoothed on some scale R. Left panel: PDF of $\hat{\mathbf{J}}\cdot\hat{\mathbf{v}}_R$ from all halos in the three suites of simulations with $M > 3\times10^{13}h^{-1}M_\odot$. Results are shown for Gaussian simulations (solid line), $p_{\rm NL} = 10^6$ (dashed lines) and $p_{\rm NL} = -10^6$ (dotted lines). The Gaussian distribution is symmetric, but we find asymmetry for the parity-breaking simulations, with some dependence on the smoothing scale R. Right panel: mean correlation averaged across eight mass bins for each suite of 500 simulations. We observe a clear nonzero signal for $p_{\rm NL} = \pm10^6$ (particularly at low masses), with a negative correlation coefficient.

approach are shown in Fig. 8. This measurement shows reduced signal to noise, which we attribute to the contamination of the velocity effect by uncorrelated effects such as the Fingers-of-God contributions. It is expected that measurements using galaxy velocities, closer still to direct observations, would also be a clean probe for parity-violating signals. However, galaxies are expected to exhibit even larger noise. To examine this, we analyzed galaxies from the CAMELS [53] simulation suite to support these statements. Unfortunately, the small size of these simulations, with boxes of side length $25h^{-1}$ Mpc, prevents a quantitative analysis. Qualitatively, variations of the cosmological parameters or the type of subgrid model in the CAMELS suite led to symmetric changes in the $\hat{J}\cdot\hat{v}_h$ distribution and so cannot mimic the parity-violating signal.

For a second probe, we correlate the halo angular momentum $\mathbf{J}$, with the $\mathbf{J}_{L,R}$ proxy defined from the smoothed initial potential ϕ and density δ, as discussed in [28,29,36,37]. This is given by

$$J_i^{\rm theory}(\mathbf{x}) = \epsilon_{ijk}\partial^j\partial^m\phi_R(\mathbf{x})\partial^k\partial_m\delta_R(\mathbf{x}),$$
$$J^i_{L,R}(\mathbf{k}) = \frac{1}{2}[(\delta^{ij}_{\rm K} - \hat{\mathbf{k}}^i\hat{\mathbf{k}}^j) \pm ie^{ijk}\hat{\mathbf{k}}_k]J_j^{\rm theory}(\mathbf{k}) \qquad (18)$$

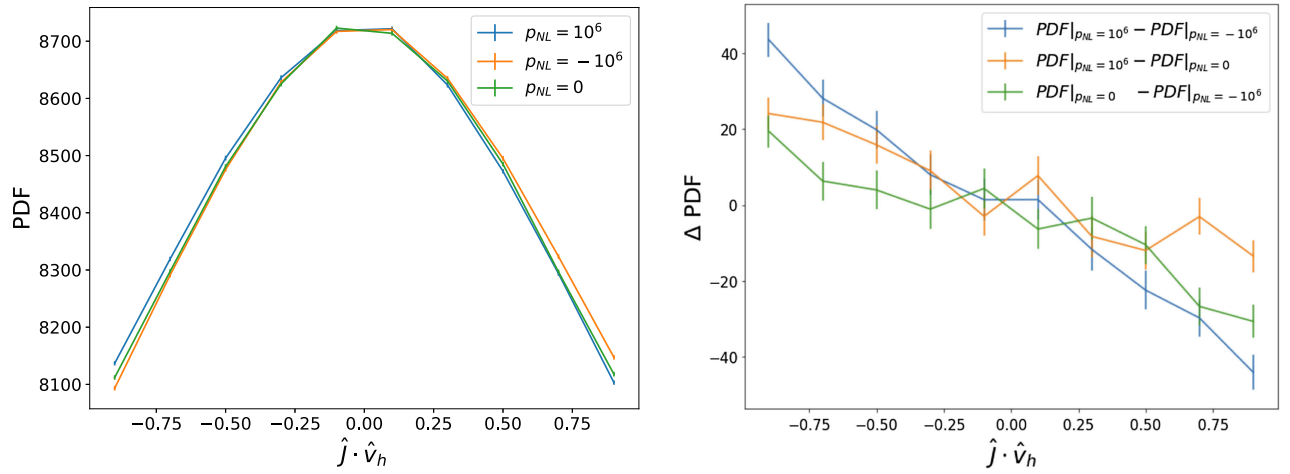

FIG. 8. Correlation between redshift zero halo angular momentum, $\mathbf{J}$, and the halo velocity, $\mathbf{v}_h$, at $z = 0$. As in Fig. 7, we plot the PDF of all the ROCKSTAR halos (left panel) and the differential change (right panel). Whilst noisier than the equivalent correlation with the initial condition velocity field, this demonstrates that the parity-violating signals can be seen using late-time measurements only.

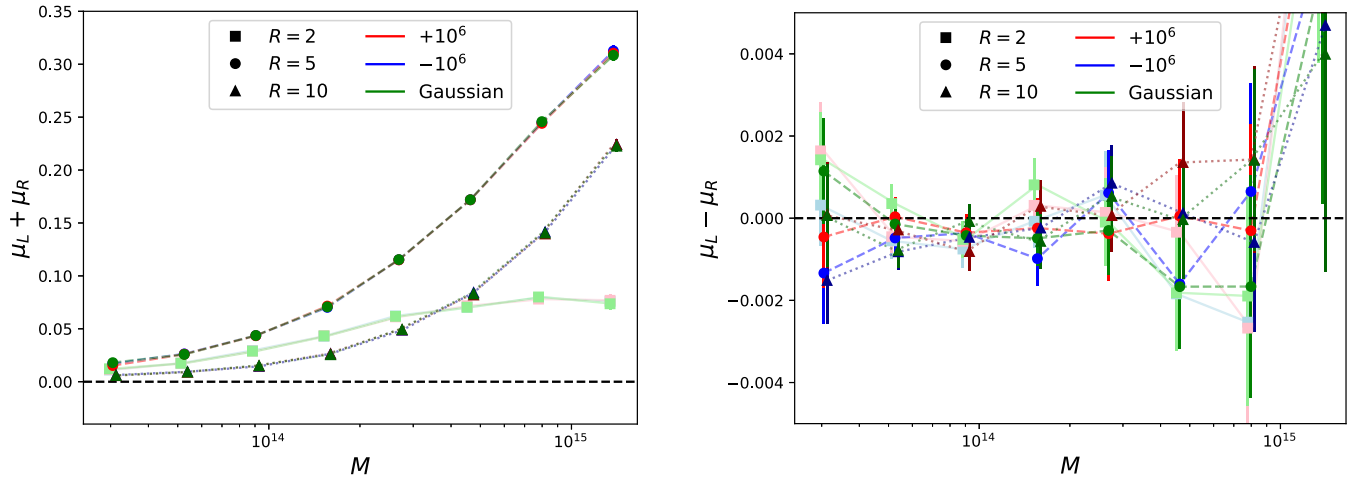

FIG. 9. Cosine between redshift zero halo angular momentum, $\mathbf{J}$, and the helical templates, $\mathbf{J}_{L,R}$ defined from the initial density field, smoothed on some scale R, with $\mu_{L,R} \equiv \hat{\mathbf{J}} \cdot \hat{\mathbf{J}}_{L,R}$. Left panel: parity-conserving contribution, $\mu_L + \mu_R$, binned in mass and averaged over 500 simulations. We find a strong correlation, matching the results of [29]; this is not seen to depend on $p_{\rm NL}$. Right panel: parity-violating contribution, $\mu_L - \mu_R$, binned as before. We find no discernible signal in this case, regardless of $p_{\rm NL}$, even though it is not nulled by symmetry arguments.

explicitly projecting onto the helical basis in the second equation. In Fig. 9, we plot the cosines $\mu_{L,R} \equiv \hat{\mathbf{J}} \cdot \hat{\mathbf{J}}_{L,R}$ for each set of simulations, and a variety of smoothing scales. The parity-conserving contributions show a clear signal, echoing the conclusion of [29]; the angular momenta of halos correlates with the primordial density field. Here, we observe largest correlations for smoothing scales $R = 5h^{-1}$ Mpc, which is somewhat larger than that suggested in [29], since the halos in our simulations are more massive and have larger Lagrangian radii. We do not observe any differences between the two sets of simulations, indicating that any contributions quadratic in $p_{\rm NL}^2$ are small. Considering $\mu_L - \mu_R$, we find no evidence for parity violation sourcing a helical angular momentum, with results consistent with zero for all values of $p_{\rm NL}$, mass bins, and smoothing. This result is not obvious *a priori*, since $\mu_L - \mu_R$ could contain terms linear in $p_{\rm NL}$ (cf. Sec. II E). We conclude that any signatures are too small to see in our choice of initial conditions, likely due to the strong scale dependence of the assumed primordial correlator.

VI. CONCLUSION

By probing the parity properties of the late-time Universe, we can place constraints on nonstandard physics occurring during inflation or low-redshift structure growth. In this work, we have performed the first numerical study of mirror asymmetries in large-scale structure by generating and analyzing simulations with a particular form of parity-violating initial conditions. This corresponds to injecting an imaginary inflationary four-point function, proportional to an amplitude $ip_{\rm NL}$, and computing various statistics on the evolved simulations at low redshift.

Our principal conclusion is that early-Universe parity violation is difficult to detect in the late Universe. Owing to homogeneity and isotropy, the realization-averaged power spectrum, bispectrum, and halo mass function are not affected by our modifications to the initial conditions, even on arbitrarily nonlinear scales and including redshift-space distortions. This has been explicitly verified with simulations, carefully accounting for parity-conserving $\mathcal{O}(p_{\rm NL}^2)$ contributions. To measure parity violation from scalar observables, we must look to four-point functions or beyond (since no lower-point functions can carry the all-important scalar triple product), such as those used in the large-scale structure analyses of [20,21], following the methodology of [22], and, the CMB analyses of [24,54]. Whilst nonlinear evolution modifies the shapes of late-time trispectra, it does not source parity-breaking correlators, and we find a clear detection of a late-Universe parity violation using a novel trispectrum estimator.

A conceptually simpler test for parity violation comes from tensorial quantities, such as the angular momentum of halos. Theoretically, parity violation can be probed using both the correlation of halo angular momenta with velocity fields (a naturally occurring pseudoscalar), and helical proxies extracted from the initial conditions [29]. In our setup, we find a strong correlation of angular momentum and velocity, scaling linearly with $p_{\rm NL}$, but no signal in the latter observable (though this is allowed theoretically). Whilst such quantities can be straightforwardly extracted from N-body simulations, the realistic measurement is a little more nuanced, since we usually have access only to projected velocity fields (themselves contaminated with nonlinear effects such as the Fingers-of-God effect), and there are nontrivial baryonic effects at play. These complications have,

to some extent, already been solved in [28,29,36,37], for example using reconstructions of the local density field, making the underlying statistic a potentially promising observable for future study.

Finally, we make publicly available our simulation suite, QUIJOTE-ODD, together with different data products such as halo catalogs and power spectra, to allow future exploration of simulations. A description of the data products and how to access them is available at https://quijote-simulations.readthedocs.io/en/latest/odd.html. We envisage that a number of other tests can be explored, for example, machine learning determinations of the subtle signatures of inflationary parity violation. Another intriguing possibility is that our primordial injection could impact galaxy intrinsic alignments, due to the correlation between galaxy shapes and local properties such as angular momenta. Though one would require hydrodynamic simulations for a full study, this could potentially lead to unexplored signals in the EB cross-correlation of galaxy shear.

ACKNOWLEDGMENTS

We thank Ue-Li Pen, Shy Genel and Jiamin Hou for enlightening conversations, and are grateful to Eiichiro Komatsu and David Spergel for comments on the manuscript, as well as Moslem Ahmadvand, Enrico Pajer and Xi Tong for feedback on the preprint. We also thank the anonymous referee for insightful feedback. All authors thank the Simons Foundation for support. This work was partly conceptualized at the "Primordial Physics with Spectroscopic Surveys" workshop in San Diego, hosted by Dan Green; the remainder stems from a bagel-fueled argument between W. R. C. and O. H. E. P.

APPENDIX A: TRISPECTRUM ESTIMATORS

Following the discussion in Sec. II, a general trispectrum of some real field δ can be written as

$$\langle\delta(\mathbf{k}_1)\cdots\delta(\mathbf{k}_4)\rangle = (2\pi)^3\delta_{\rm D}(\mathbf{k}_1+\mathbf{k}_2+\mathbf{k}_3+\mathbf{k}_4)[\tau_+(k_1,k_2,k_3,k_4,K,K')+i(\mathbf{k}_1\cdot\mathbf{k}_2\times\mathbf{k}_3)\tau_-(k_1,k_2,k_3,k_4,K,K')], \quad \text{(A1)}$$

where $\tau_\pm$ give parity-even and parity-odd components, and we have factorized out the scalar triple product in the latter. Each component depends on four side lengths (k_i) and two diagonals ($K \equiv |\mathbf{k}_1+\mathbf{k}_2|$ and $K' \equiv |\mathbf{k}_1+\mathbf{k}_3|$); in practice, it is necessary to parametrize by only one diagonal, else the trispectrum estimators are not separable. Below, we consider how to estimate each component, and, in Appendix B, relate this to theoretical trispectra. The parity-even estimator is additionally described in [55].

1. Parity-even estimator

Considering bins q_i in $\mathbf{k}_i$ and Q in $\mathbf{K}$, a general estimator for the parity-even component is given by

$$\hat{T}_+(q_1,q_2,q_3,q_4,Q) \propto \int_{\mathbf{k}_i\in q_i,\mathbf{K}\in Q}\left[\prod_{i=1}^4\delta(\mathbf{k}_i)\right](2\pi)^3\delta_{\rm D}(\mathbf{k}_1+\mathbf{k}_2-\mathbf{K})(2\pi)^3\delta_{\rm D}(\mathbf{k}_3+\mathbf{k}_4+\mathbf{K}), \quad \text{(A2)}$$

where we explicitly integrate over the internal momentum $\mathbf{K}$ and drop a normalization factor. This can be efficiently implemented by rewriting the Dirac deltas as exponential integrals, yielding

$$\begin{aligned}\hat{T}_+(q_1,q_2,q_3,q_4,Q) \propto \int_{\mathbf{K}\in Q}&\left[\int d\mathbf{x}\left(\int_{\mathbf{k}_1\in q_1}\delta(\mathbf{k}_1)e^{-i\mathbf{k}_1\cdot\mathbf{x}}\right)\left(\int_{\mathbf{k}_2\in q_2}\delta(\mathbf{k}_2)e^{-i\mathbf{k}_2\cdot\mathbf{x}}\right)e^{i\mathbf{K}\cdot\mathbf{x}}\right]\\ &\times\left[\int d\mathbf{y}\left(\int_{\mathbf{k}_3\in q_3}\delta(\mathbf{k}_3)e^{-i\mathbf{k}_3\cdot\mathbf{y}}\right)\left(\int_{\mathbf{k}_4\in q_4}\delta(\mathbf{k}_4)e^{-i\mathbf{k}_4\cdot\mathbf{y}}\right)e^{-i\mathbf{K}\cdot\mathbf{y}}\right]. \quad \text{(A3)}\end{aligned}$$

Practical computation is achieved via repeated Fourier transforms, first computing the N_k transforms of δ (for N_k bins), then assembling the $N_k(N_k+1)/2$ pairs (from the $\mathbf{x}$, $\mathbf{y}$ integrals), and lastly summing over $\mathbf{K}$ for all Q bins of interest. The typical normalization includes the same functions but with the $\delta(\mathbf{k})$ fields replaced with unity, such that the normalization counts the total number of tetrahedra in a given bin.

The above estimator has the following symmetries:

$$\hat{T}_+(q_1,q_2,q_3,q_4,Q) = \hat{T}_+(q_2,q_1,q_3,q_4,Q) = \hat{T}_+(q_3,q_4,q_1,q_2,Q); \quad \text{(A4)}$$

in addition, modes with $\hat{T}_+(q_1,q_3,q_2,q_4,Q)$ are partially covariant with $\hat{T}_+(q_1,q_2,q_3,q_4,Q)$, due to the labeling degeneracy of the internal (diagonal) momentum. Via the triangle conditions on $\mathbf{k}_i,\mathbf{K}$, nontrivial components are specified by

$$q_1 \le q_2, \qquad q_3 \le q_4, \qquad q_1 \le q_3, \qquad |q_1 - q_2| \le Q \le q_1 + q_2, \qquad |q_3 - q_4| \le Q \le q_3 + q_4. \tag{A5}$$

2. Parity-odd estimator

To estimate the parity-odd trispectrum components, we use a similar scheme, but insert a factor of $\mathbf{k}_1 \cdot \mathbf{k}_2 \times \mathbf{k}_3$ to pick out only the imaginary component:

$$\hat{T}_-(q_1, q_2, q_3, q_4, Q) \propto \int_{\mathbf{k}_i \in q_i, \mathbf{K} \in Q} \left[\prod_{i=1}^{4} \delta(\mathbf{k}_i)\right] (2\pi)^3 \delta_{\rm D}(\mathbf{k}_1 + \mathbf{k}_2 - \mathbf{K})(2\pi)^3 \delta_{\rm D}(\mathbf{k}_3 + \mathbf{k}_4 + \mathbf{K})\, (\mathbf{k}_1 \cdot \mathbf{k}_2 \times \mathbf{k}_3). \tag{A6}$$

Note that parity-even contributions are nulled in this estimator due to $\mathbf{k} \to -\mathbf{k}$ labeling symmetries. To form a practical estimator, the triple product can be rewritten as a Cartesian sum, leading to

$$\begin{aligned}\hat{T}_-(q_1, q_2, q_3, q_4, Q) \propto \epsilon_{ijk} \int_{\mathbf{K} \in Q} \left[\int d\mathbf{x} \left(\int_{\mathbf{k}_1 \in q_1} k_1^i \delta(\mathbf{k}_1) e^{-i\mathbf{k}_1 \cdot \mathbf{x}}\right) \left(\int_{\mathbf{k}_2 \in q_2} k_2^j \delta(\mathbf{k}_2) e^{-i\mathbf{k}_2 \cdot \mathbf{x}}\right) e^{i\mathbf{K} \cdot \mathbf{x}}\right] \\ \times \left[\int d\mathbf{y} \left(\int_{\mathbf{k}_3 \in q_3} k_3^k \delta(\mathbf{k}_3) e^{-i\mathbf{k}_3 \cdot \mathbf{y}}\right) \left(\int_{\mathbf{k}_4 \in q_4} \delta(\mathbf{k}_4) e^{-i\mathbf{k}_4 \cdot \mathbf{y}}\right) e^{-i\mathbf{K} \cdot \mathbf{y}}\right].\end{aligned} \tag{A7}$$

This is computed similarly to before, but now requires computing four Fourier transforms per k bin (for $i = 1, 2, 3$ and without $\mathbf{k}$). The normalization factor is defined as for the even case, without the triple product, though the particular choice is, to an extent, arbitrary.

An alternative (but equivalent) approach to compute the estimator is to expand the triple product in spherical harmonics, via the standard relation

$$\mathbf{k}_1 \cdot \mathbf{k}_2 \times \mathbf{k}_3 = -\sqrt{6} i \left(\frac{4\pi}{3}\right)^{3/2} k_1 k_2 k_3 \sum_{m_1 m_2 m_3} \begin{pmatrix} 1 & 1 & 1 \\ m_1 & m_2 & m_3 \end{pmatrix} Y_{1m_1}(\hat{\mathbf{k}}_1) Y_{1m_2}(\hat{\mathbf{k}}_2) Y_{1m_3}(\hat{\mathbf{k}}_3). \tag{A8}$$

This separates the $\mathbf{k}_i$ dependence, allowing for the estimator to be written as

$$\begin{aligned}\hat{T}_-(q_1, q_2, q_3, q_4, Q) \propto -\sqrt{6} i \left(\frac{4\pi}{3}\right)^{3/2} \sum_{m_1 m_2 m_3} \begin{pmatrix} 1 & 1 & 1 \\ m_1 & m_2 & m_3 \end{pmatrix} \\ \times \int_{\mathbf{K} \in Q} \left[\int d\mathbf{x} \left(\int_{\mathbf{k}_1 \in q_1} k_1 Y_{1m_1}(\hat{\mathbf{k}}_1) \delta(\mathbf{k}_1) e^{-i\mathbf{k}_1 \cdot \mathbf{x}}\right) \left(\int_{\mathbf{k}_2 \in q_2} k_2 Y_{1m_2}(\hat{\mathbf{k}}_2) \delta(\mathbf{k}_2) e^{-i\mathbf{k}_2 \cdot \mathbf{x}}\right) e^{i\mathbf{K} \cdot \mathbf{x}}\right] \\ \times \left[\int d\mathbf{y} \left(\int_{\mathbf{k}_3 \in q_3} k_3 Y_{1m_3}(\hat{\mathbf{k}}_3) \delta(\mathbf{k}_3) e^{-i\mathbf{k}_3 \cdot \mathbf{y}}\right) \left(\int_{\mathbf{k}_4 \in q_4} \delta(\mathbf{k}_4) e^{-i\mathbf{k}_4 \cdot \mathbf{y}}\right) e^{-i\mathbf{K} \cdot \mathbf{y}}\right],\end{aligned} \tag{A9}$$

for $m_i \in \{-1, 0, 1\}$ and $m_1 + m_2 + m_3 = 0$. This again requires four FFTs per k bin, though only a total of seven terms need to be combined together.

The above estimator has various symmetry properties:

$$\hat{T}_-(q_1, q_2, q_3, q_4, Q) = -\hat{T}_-(q_2, q_1, q_3, q_4, Q) = \hat{T}_-(q_3, q_4, q_1, q_2, Q) \tag{A10}$$

(noting the negative sign under $q_1 \leftrightarrow q_2$ or $q_3 \leftrightarrow q_4$ interchange); as before, modes with $\hat{T}_-(q_1, q_3, q_2, q_4, Q)$ are partially covariant with $\hat{T}_-(q_1, q_2, q_3, q_4, Q)$, due to the labeling degeneracy of the internal (diagonal) momentum. Finally we note that, if $q_1 = q_2$ or $q_3 = q_4$, the trispectrum must vanish, based on the above symmetries. This modifies the condition for nontrivial bins to

$$q_1 < q_2, \qquad q_3 < q_4, \qquad q_1 \le q_3, \qquad |q_1 - q_2| \le Q \le q_1 + q_2, \qquad |q_3 - q_4| \le Q \le q_3 + q_4, \tag{A11}$$

and one can additionally impose $q_2 \le q_4$ if $q_1 = q_3$.

APPENDIX B: THEORETICAL PRIMORDIAL TRISPECTRA

In the below, we consider how to relate the above trispectrum estimators to theoretical models, i.e. to compute the expectation of $T_\pm$ for a given model for $\langle\delta(\mathbf{k}_1)\cdots\delta(\mathbf{k}_4)\rangle$, specified by $\tau_\pm$, as in (A1).

1. Parity-even trispectrum

In expectation, the parity-even trispectrum estimator yields

$$\mathbb{E}[\hat{T}_+(q_1,q_2,q_3,q_4,Q)] \propto \int_{\mathbf{k}_i\in q_i,\mathbf{K}\in Q} \tau_+(k_1,k_2,k_3,k_4,K,K')(2\pi)^3\delta_{\rm D}(\mathbf{k}_1+\mathbf{k}_2-\mathbf{K})\,(2\pi)^3\delta_{\rm D}(\mathbf{k}_3+\mathbf{k}_4+\mathbf{K}). \tag{B1}$$

Assuming τ_+ to be independent of the second diagonal $K'\equiv|\mathbf{k}_1+\mathbf{k}_3|$, this can be simplified by rewriting the Dirac deltas as exponentials and using the result $\int_{\hat{\mathbf{k}}} e^{-i\mathbf{k}\cdot\mathbf{x}} = j_0(kx)$:

$$\begin{aligned}\mathbb{E}[\hat{T}_+(q_1,q_2,q_3,q_4,Q)] \propto \int_{k_i\in q_i,K\in Q} &\tau_+(k_1,k_2,k_3,k_4,K)\\ &\times\left(4\pi\int x^2dx j_0(k_1x)j_0(k_2x)j_0(Kx)\right)\left(4\pi\int y^2dy j_0(k_3y)j_0(k_4y)j_0(Ky)\right).\end{aligned} \tag{B2}$$

Further noting that

$$4\pi\int x^2dx j_0(ax)j_0(bx)j_0(cx) = \frac{\pi^2}{abc}\Delta(a,b,c), \tag{B3}$$

where $\Delta=1$ if $\{a,b,c\}$ obey triangle conditions and zero otherwise, this can be written as

$$\mathbb{E}[\hat{T}_+(q_1,q_2,q_3,q_4,Q)] \propto \int_{k_i\in q_i,K\in Q} \frac{\pi^4}{(k_1k_2k_3k_4)K^2}\tau_+(k_1,k_2,k_3,k_4,K)\Delta(k_1,k_2,K)\Delta(k_3,k_4,K), \tag{B4}$$

where the factors of Δ can be dropped if all modes in the bin obey triangle conditions. The normalization is identical, except without the factor of τ_+.

In the thin-bin limit, we can drop the k_i and K integrals, giving a normalization of $q_1q_2q_3q_4(\delta k)^5/(32\pi^6)$, and thus the full trispectrum

$$\mathbb{E}[\hat{T}_+(q_1,q_2,q_3,q_4,Q)] \approx \tau_+(q_1,q_2,q_3,q_4,Q). \tag{B5}$$

In the limit of a K'-independent τ_+, the parity-even trispectrum is thus an unbiased estimator of τ_+ in the thin-bin limit.

2. Parity-odd trispectrum

A similar procedure can be performed for the parity-odd trispectrum estimator, starting from the general form

$$\begin{aligned}\mathbb{E}[\hat{T}_-(q_1,q_2,q_3,q_4,Q)] \equiv i\int_{\mathbf{k}_i\in q_i,\mathbf{K}\in Q} &(\mathbf{k}_1\cdot\mathbf{k}_2\times\mathbf{k}_3)^2\tau_-(k_1,k_2,k_3,k_4,K,K')\\ &\times(2\pi)^3\delta_{\rm D}(\mathbf{k}_1+\mathbf{k}_2-\mathbf{K})(2\pi)^3\delta_{\rm D}(\mathbf{k}_3+\mathbf{k}_4+\mathbf{K}).\end{aligned} \tag{B6}$$

To simplify this, we first rewrite the squared triple product in spherical harmonics, starting from (A8)

$$\begin{aligned}(\hat{\mathbf{k}}_1\cdot\hat{\mathbf{k}}_2\times\hat{\mathbf{k}}_3)^2 = -6(4\pi)^{3/2}\sum_{L_iM_i} &Y_{L_1M_1}(\hat{\mathbf{k}}_1)Y_{L_2M_2}(\hat{\mathbf{k}}_2)Y_{L_3M_3}(\hat{\mathbf{k}}_3)\begin{pmatrix}L_1 & L_2 & L_3\\ M_1 & M_2 & M_3\end{pmatrix}\\ &\times\begin{pmatrix}1&1&L_1\\0&0&0\end{pmatrix}\begin{pmatrix}1&1&L_2\\0&0&0\end{pmatrix}\begin{pmatrix}1&1&L_3\\0&0&0\end{pmatrix}\sqrt{(2L_1+1)(2L_2+1)(2L_3+1)}\begin{Bmatrix}L_1&L_2&L_3\\1&1&1\\1&1&1\end{Bmatrix},\end{aligned} \tag{B7}$$

where $L_i \in \{0,2\}$ and we have used the product identity of spherical harmonics as well as the definition of the Wigner $9j$ symbol. Next, we rewrite the Dirac deltas as exponentials and perform the $\hat{\mathbf{k}}_i$ integrals via $\int_{\hat{\mathbf{k}}} e^{\pm i\mathbf{k}\cdot\mathbf{x}} Y_{LM}(\hat{\mathbf{k}}) = i^{\pm L} j_L(kx) Y_{LM}(\hat{\mathbf{x}})$. Assuming the trispectrum to be K' independent, as before, this yields

$$\begin{aligned}\mathbb{E}[\hat{T}_-(q_1,q_2,q_3,q_4,Q)] \propto -6i(4\pi)^{1/2} &\int_{k_i\in q_i, K\in Q} k_1^2 k_2^2 k_3^2 \tau_-(k_1,k_2,k_3,k_4,K) \\ &\times \sum_{L_i M_i} \left(4\pi \int x^2 dx j_{L_1}(k_1 x) j_{L_2}(k_2 x) j_{L_3}(Kx)\right) i^{-L_1-L_2-L_3} \begin{pmatrix} L_1 & L_2 & L_3 \\ M_1 & M_2 & M_3 \end{pmatrix} \\ &\times \left(\int d\hat{\mathbf{x}}\, Y_{L_1M_1}(\hat{\mathbf{x}}) Y_{L_2M_2}(\hat{\mathbf{x}}) Y_{L_3M_3}(\hat{\mathbf{x}})\right)\left(4\pi \int y^2 dy j_{L_3}(k_3 y) j_0(k_4 y) j_{L_3}(Ky)\right) \\ &\times \begin{pmatrix} 1 & 1 & L_1 \\ 0 & 0 & 0 \end{pmatrix}\begin{pmatrix} 1 & 1 & L_2 \\ 0 & 0 & 0 \end{pmatrix}\begin{pmatrix} 1 & 1 & L_3 \\ 0 & 0 & 0 \end{pmatrix}\sqrt{(2L_1+1)(2L_2+1)(2L_3+1)}\begin{Bmatrix} L_1 & L_2 & L_3 \\ 1 & 1 & 1 \\ 1 & 1 & 1 \end{Bmatrix}, \end{aligned} \tag{B8}$$

where we have integrated over $\hat{\mathbf{y}}$ then $\hat{\mathbf{K}}$. All k_i and K integrals are performed with respect to the Lebesgue measure $k^2 dk/(2\pi^2)$. Finally, we note that the $\hat{\mathbf{x}}$ integral is a Gaunt factor, and use $3j$ completeness to yield the result

$$\begin{aligned}\mathbb{E}[\hat{T}_-(q_1,q_2,q_3,q_4,Q)] \propto -6i &\int_{k_i\in q_i, K\in Q} k_1^2 k_2^2 k_3^2 \tau_-(k_1,k_2,k_3,k_4,K) \sum_{L_1L_2L_3} (2L_1+1)(2L_2+1)(2L_3+1) \\ &\times i^{-L_1-L_2-L_3}\begin{pmatrix} L_1 & L_2 & L_3 \\ 0 & 0 & 0 \end{pmatrix}\begin{pmatrix} 1 & 1 & L_1 \\ 0 & 0 & 0 \end{pmatrix}\begin{pmatrix} 1 & 1 & L_2 \\ 0 & 0 & 0 \end{pmatrix}\begin{pmatrix} 1 & 1 & L_3 \\ 0 & 0 & 0 \end{pmatrix}\begin{Bmatrix} L_1 & L_2 & L_3 \\ 1 & 1 & 1 \\ 1 & 1 & 1 \end{Bmatrix} \qquad \text{(B9)} \\ &\times \left(4\pi \int x^2 dx j_{L_1}(k_1 x) j_{L_2}(k_2 x) j_{L_3}(Kx)\right)\left(4\pi \int y^2 dy j_{L_3}(k_3 y) j_0(k_4 y) j_{L_3}(Ky)\right). \qquad \text{(B10)} \end{aligned}$$

This is just a collection of coupled one-dimensional integrals, and the full spectrum can be evaluated with two-dimensional quadrature. We note that the x and y integrals are analytic, taking the form [56]

$$\begin{aligned}4\pi \int x^2 dx j_{\ell_1}(ax) j_{\ell_2}(bx) j_{\ell_3}(cx) = \frac{\pi^2}{abc}\Delta(a,b,c)&\begin{pmatrix} \ell_1 & \ell_2 & \ell_3 \\ 0 & 0 & 0 \end{pmatrix}^{-1} i^{\ell_1+\ell_2-\ell_3}\sqrt{2\ell_3+1}\left(\frac{a}{c}\right)^{\ell_3} \\ &\times \sum_{L=0}^{\ell_3}\begin{pmatrix} 2\ell_3 \\ 2L \end{pmatrix}^{1/2}\left(\frac{b}{a}\right)^L \sum_{\ell'=|\ell_2-L|}^{\ell_2+L}(2\ell'+1)\begin{pmatrix} \ell_1 & \ell_3-L & \ell' \\ 0 & 0 & 0 \end{pmatrix}\begin{pmatrix} \ell_2 & L & \ell' \\ 0 & 0 & 0 \end{pmatrix} \\ &\times \begin{Bmatrix} \ell_1 & \ell_2 & \ell_3 \\ L & \ell_3-L & \ell' \end{Bmatrix} L_{\ell'}\left(\frac{a^2+b^2-c^2}{2ab}\right), \end{aligned} \tag{B11}$$

where L_ℓ is a Legendre polynomial, and Δ ensures triangle conditions, as before. This involves both $3j$ and $6j$ Wigner symbols, and here requires only $\ell_i \in \{0,2\}$. The y integrals always involve $\ell_3 = 0$, yielding

$$4\pi \int y^2 dy j_\ell(Ky) j_\ell(k_3 y) j_0(k_4 y) = \frac{\pi^2}{k_3 k_4 K}\Delta(k_3,k_4,K) L_\ell\left(\frac{K^2+k_3^2-k_4^2}{2Kk_3}\right), \tag{B12}$$

where $\ell \in \{0,2\}$ is required. We note that this makes the separability in $\{k_3,k_4,K\}$ less trivial (though still sum separable, since the Legendre functions are polynomial).

In the thin-bin limit, we can write

$$\mathbb{E}[\hat{T}_-(q_1,q_2,q_3,q_4,Q)] \approx -\frac{6}{\pi^2} i q_1^3 q_2^3 q_3^2 Q \tau_-(q_1,q_2,q_3,q_4,Q) \sum_{L_1 L_2 L_3} i^{-L_1-L_2-L_3}(2L_1+1)(2L_2+1)(2L_3+1)$$
$$\times \begin{pmatrix} L_1 & L_2 & L_3 \\ 0 & 0 & 0 \end{pmatrix} \begin{pmatrix} 1 & 1 & L_1 \\ 0 & 0 & 0 \end{pmatrix} \begin{pmatrix} 1 & 1 & L_2 \\ 0 & 0 & 0 \end{pmatrix} \begin{pmatrix} 1 & 1 & L_3 \\ 0 & 0 & 0 \end{pmatrix} \begin{Bmatrix} L_1 & L_2 & L_3 \\ 1 & 1 & 1 \\ 1 & 1 & 1 \end{Bmatrix}$$
$$\times \left(4\pi \int x^2 dx j_{L_1}(q_1 x) j_{L_2}(q_2 x) j_{L_3}(Q x)\right) L_{L_3}\left(\frac{Q^2+q_3^2-q_4^2}{2Q q_3}\right), \tag{B13}$$

assuming triangle conditions to be satisfied. This is much more complex than the parity-even equivalent (B5), due to the $(\mathbf{k}_1 \cdot \mathbf{k}_2 \times \mathbf{k}_3)^2$ factor. If this was additionally included in the normalization, the limit would be simply $i\tau_-(q_1,q_2,q_3,q_4,Q)$; however, this is likely to be unstable for close-to-coplanar tetrahedral configurations, whence $(\mathbf{k}_1 \cdot \mathbf{k}_2 \times \mathbf{k}_3)^2$ vanishes.

[1] C. S. Wu, E. Ambler, R. W. Hayward, D. D. Hoppes, and R. P. Hudson, Phys. Rev. **105**, 1413 (1957).
[2] T. D. Lee and C. N. Yang, Phys. Rev. **104**, 254 (1956).
[3] T. Liu, X. Tong, Y. Wang, and Z.-Z. Xianyu, J. High Energy Phys. 04 (2020) 189.
[4] G. Cabass, S. Jazayeri, E. Pajer, and D. Stefanyszyn, J. High Energy Phys. 02 (2023) 021.
[5] L. Bordin and G. Cabass, J. Cosmol. Astropart. Phys. 07 (2020) 014.
[6] A. Lue, L. Wang, and M. Kamionkowski, Phys. Rev. Lett. **83**, 1506 (1999).
[7] L. Sorbo, J. Cosmol. Astropart. Phys. 06 (2011) 003.
[8] N. Bartolo, S. Matarrese, M. Peloso, and M. Shiraishi, J. Cosmol. Astropart. Phys. 01 (2015) 027.
[9] N. Bartolo, S. Matarrese, M. Peloso, and M. Shiraishi, J. Cosmol. Astropart. Phys. 07 (2015) 039.
[10] N. Bartolo and G. Orlando, J. Cosmol. Astropart. Phys. 07 (2017) 034.
[11] M. Shiraishi, Phys. Rev. D **94**, 083503 (2016).
[12] M. Biagetti and G. Orlando, J. Cosmol. Astropart. Phys. 07 (2020) 005.
[13] V. Gluscevic and M. Kamionkowski, Phys. Rev. D **81**, 123529 (2010).
[14] M. H. G. Lee, C. McCulloch, and E. Pajer, J. High Energy Phys. 11 (2023) 038.
[15] A. D. Sakharov, J. Exp. Theor. Phys. Lett. **5**, 24 (1967).
[16] S. Alexander and N. Yunes, Phys. Rep. **480**, 1 (2009).
[17] S. Alexander, A. Marcianò, and D. Spergel, J. Cosmol. Astropart. Phys. 04 (2013) 046.
[18] S. Alexander, Int. J. Mod. Phys. D **25**, 1640013 (2016).
[19] S. H. Alexander, M. E. Peskin, and M. M. Sheikh-Jabbari, Phys. Rev. Lett. **96**, 081301 (2006).
[20] O. H. E. Philcox, Phys. Rev. D **106**, 063501 (2022).
[21] J. Hou, Z. Slepian, and R. N. Cahn, Mon. Not. R. Astron. Soc. **522**, 5701 (2023).
[22] R. N. Cahn, Z. Slepian, and J. Hou, Phys. Rev. Lett. **130**, 201002 (2023).
[23] G. Cabass, M. M. Ivanov, and O. H. E. Philcox, Phys. Rev. D **107**, 023523 (2023).
[24] O. H. E. Philcox, Phys. Rev. Lett. **131**, 181001 (2023).
[25] A. Aghamousa, J. Aguilar, S. Ahlen, S. Alam, L. E. Allen, C. Allende Prieto, J. Annis, S. Bailey *et al.* (DESI Collaboration), arXiv:1611.00036.
[26] R. Laureijs, J. Amiaux, S. Arduini, J. L. Augueres, J. Brinchmann, R. Cole, M. Cropper, C. Dabin, L. Duvet *et al.*, arXiv:1110.3193.
[27] D. J. Schlegel *et al.*, arXiv:2209.04322.
[28] P. Motloch, H.-R. Yu, U.-L. Pen, and Y. Xie, Nat. Astron. **5**, 283 (2021).
[29] H.-R. Yu, P. Motloch, U.-L. Pen, Y. Yu, H. Wang, H. Mo, X. Yang, and Y. Jing, Phys. Rev. Lett. **124**, 101302 (2020).
[30] F. Villaescusa-Navarro *et al.*, Astrophys. J. Suppl. Ser. **250**, 2 (2020).
[31] M. Shiraishi, J. Cosmol. Astropart. Phys. 06 (2012) 015.
[32] K. W. Masui, U.-L. Pen, and N. Turok, Phys. Rev. Lett. **118**, 221301 (2017).
[33] N. Aghanim *et al.* (Planck Collaboration), Astron. Astrophys. **596**, A110 (2016).
[34] G. Orlando, J. Cosmol. Astropart. Phys. 12 (2022) 019.
[35] Y. Minami and E. Komatsu, Phys. Rev. Lett. **125**, 221301 (2020).
[36] P. Motloch, U.-L. Pen, and H.-R. Yu, Phys. Rev. D **105**, 083504 (2022).
[37] P. Motloch, U.-L. Pen, and H.-R. Yu, Phys. Rev. D **105**, 083512 (2022).
[38] H. Jia, H.-M. Zhu, and U.-L. Pen, Astrophys. J. **943**, 32 (2023).
[39] R. Scoccimarro, L. Hui, M. Manera, and K. C. Chan, Phys. Rev. D **85**, 083002 (2012).
[40] F. Villaescusa-Navarro *et al.*, Astrophys. J. Suppl. Ser. **250**, 2 (2020).

[41] W. R. Coulton, F. Villaescusa-Navarro, D. Jamieson, M. Baldi, G. Jung, D. Karagiannis, M. Liguori, L. Verde, and B. D. Wandelt, Astrophys. J. **943**, 64 (2023).
[42] https://quijote-simulations.readthedocs.io.
[43] A. Lewis, A. Challinor, and A. Lasenby, Astrophys. J. **538**, 473 (2000).
[44] V. Springel, Mon. Not. R. Astron. Soc. **364**, 1105 (2005).
[45] M. Davis, G. Efstathiou, C. S. Frenk, and S. D. M. White, Astrophys. J. **292**, 371 (1985).
[46] P. S. Behroozi, R. H. Wechsler, and H.-Y. Wu, Astrophys. J. **762**, 109 (2013).
[47] R. W. Hockney and J. W. Eastwood, *Computer Simulation Using Particles* (Taylor & Francis, Abingdon, 1981).
[48] F. Villaescusa-Navarro, Pylians: Python libraries for the analysis of numerical simulations, Astrophysics Source Code Library, record ascl:1811.008, 2018.
[49] W. R. Coulton, F. Villaescusa-Navarro, D. Jamieson, M. Baldi, G. Jung, D. Karagiannis, M. Liguori, L. Verde, and B. D. Wandelt, Astrophys. J. **943**, 178 (2023).
[50] G. Jung, A. Ravenni, M. Baldi, W. R. Coulton, D. Jamieson, D. Karagiannis, M. Liguori, H. Shao, L. Verde, F. Villaescusa-Navarro, and B. D. Wandelt, arXiv:2305.10597.
[51] S. Foreman, W. Coulton, F. Villaescusa-Navarro, and A. Barreira, Mon. Not. R. Astron. Soc. **498**, 2887 (2020).
[52] P. S. Behroozi, R. H. Wechsler, and H.-Y. Wu, Astrophys. J. **762**, 109 (2013).
[53] F. Villaescusa-Navarro *et al.*, Astrophys. J. **915**, 71 (2021).
[54] O. H. E. Philcox and M. Shiraishi, arXiv:2308.03831.
[55] G. Jung *et al.*, Astrophys. J. **957**, 1 (2023).
[56] R. Mehrem, J. T. Londergan, and M. H. Macfarlane, J. Phys. A **24**, 1435 (1991).